Norges miljø- og
biovitenskapelige
universitet

Master's Thesis 2017 60 ECTS
Faculty of Chemistry, Biotechnology and Food Science

Identification of a novel function of Tankyrase: Inhibition of Tankyrase catalytic activity leads to increased cellular cholesterol levels.

Caroline Zedell
Chemistry and Biotechnology, Molecular Biology

Abstrakt

Tankyrase 1 og 2 er multifunksjonelle proteiner som har viktige roller i mange cellulære prosesser. Den mest studerte funskjonen av tankyrase er regularingen av WNT/β-catenin signalveien og tankyraseinhibitorer utforskes som en terapautisk strategi for WNT/β-catenin drevet kreft. For sikker utvikling av tankyraseinhibitorer som terapuatiske midler er det viktig at alle potensielle effekter som tankyrase inhibering kan forårsake i målcellene er godt karakterisert. I denne studien ble cellulære effekter av tankyraseinhibitoren G007-LK analysert i tarmkreft cellelinjen RKO hvor vekst ikke blir påvirket av G007-LK behandling. Analyse av RNA sekvenserings data viste at behandling med G007-LK på RKO celler resulterte i oppregulert transkripsjon av gener involvert i kolesterol biosyntese. Måling av cellulære kolesterolnivåer viste at RKO celler behandlet med G007-LK inneholdt økte mengder kolesterol. Analyse av funskjonelle konsekvenser av økte kolesterolnivåer viste at RKO celler behandlet med G007-LK hadde økt antall lipid rafts i plasma membranen og økte cellulære nivåer av 24S-hydroksykolesterol og 25-hydroksykolesterol.

Samlet sett har dette arbeidet vist at inhibering av tankyrase ved G007-LK øker de cellulære kolesterol nivåene i RKO celler og det er for første gang sett en mulig sammenheng mellom tankyraseaktivitet og regulering av cellulære kolesterol nivåer.

Abstract

Tankyrases are multifunctional proteins that have important roles in many cellular processes. The most studied function of tankyrase is regulation of WNT/β-catenin signaling pathway and tankyrase inhibitors are explored as a therapeutic strategy for WNT/β-catenin driven cancers. For safe development of tankyrase inhibitors as therapeutic agents it is important that all potential effects that tankyrase inhibition might cause on the targeted cells are well characterized. In this work the cellular effect of the tankyrase inhibitor G007-LK was analyzed in the colorectal cancer RKO cell line that is insensitive to growth inhibition by G007-LK treatment. Analysis of RNA sequencing data showed that G007-LK treatment of RKO cells resulted in up regulated transcription of genes involved in cholesterol biosynthesis. Measurement of cellular cholesterol levels revealed that G007-LK treated RKO cells contained increased amounts of cholesterol. Analysis of functional consequences of the increased cholesterol levels showed that G007-LK treated RKO cells had increased amounts of lipid rafts in the plasma membrane and increased cellular levels of 24S-hydroxycholesterol and 25-hydroxycholesterol.

Altogether, this work have shown that inhibition of tankyrase by G007-LK increases the cellular cholesterol levels in RKO cells and presents for the first time a possible link between tankyrase activity and regulation of cellular cholesterol levels.

Acknowledgments

This thesis has been performed at professor Stefan Krauss group; Unit for Cell Signaling, Department of Microbiology at Oslo University Hospital in the period January to December 2017.

I want to thank my main supervisor Stefan Krauss for the opportunity to be a part of his research group and for expert advice through this thesis. I especially want to thank my co-supervisor Petter Angell Olsen who made this year very exciting and educational. I would also thank him for excellent guidance and support during the study.

I will also thank my internal supervisor Harald Carlsen for guidance in the writing process.

I want to thank Martin Strand for good help with the RNA sequencing data. I also want to thank Hanne Røberg-Larsen for help with analysis of oxysterols. For the fantastic social environment in the office and support through the year I want to thank Jo Waaler, Kaja Lund, Nina Solberg, Line Mygland, Shoshy Mahmuda, Max Lycke, Maria Melheim, Ida Johnsen and Elisabeth Dybing.

I would also thank my sister, my two brothers, and especially my mom and dad for always have faith in me and give me motivation to always do my best. I will also thank my friends for your support and motivational words. At last I will thank my incredibly kind and patient boyfriend Niklas Vangen, you`ve got me on other thoughts and made the year fantastic.

Oslo, Norway, December 2017

Caroline Zedell

List of Abbreviations

ABCA1	ABC transporter A1
acetyl-CoA	acetyl coenzyme A
APC	adenomatous polyposis coli tumor-suppressor gene
ADPr	ADP-ribose
ARTD	ADP-ribosyltransferase
ARC	ankyrin repeat clusters
apoA-I	apolipoprotein A-I
ABC	ATP-binding cassette
CK1	casein kinase 1
CPAP	centrosomal P4.1-associated protein
CRC	Colorectal cancer
DMSO	Dimethyl sulfoxide
DVL	Disheveled
DSB	DNA double-strand break
DNA-PK	DNA-dependent protein kinase
DNA-PKcs	DNA-dependent protein kinase catalytic subunit
ER	endoplasmic reticulum
FAP	Familial Adenomatous Polyposis
FBS	Fetal bovine serum
GLUT4	glucose transporter type 4
GSVs	GLUT4 storage vesicles
GAPDH	Glyceraldehyde-3-phosphate dehydrogenase
GSK3β	glycogen synthase kinase 3β
HDL	high-density lipoprotein
HPS	His, Pro and Ser
HDAC	histone deacetylases
HMG-CoA	hydroxymethylglutaryl CoA
HMG-CoAR	hydroxymethylglutaryl CoA reductase
IRAP	insulin responsive amino peptidase
INSIG	insulin-induced gene
ATM	kinase ataxia-telangiectasia mutated
KIF1a	kinesin family member 1a

LDLR	LDL receptors
LCAT	lecithin:cholesterol acyl transferase
LTP	lipid transfer proteins
LRP5/6	lipoprotein receptor protein 5/6
LDL	low-density lipoprotein
VLDL	low-density lipoprotein
Miki	mitotic kinetics regulator
NAD+	nicotinamide adenine dinucleotide
NHEJ	Non-homologous end joining
NFATc1	nuclear factor of activated T cells c1
NuMA	nuclear mitotic apparatus protein
PBS	Phosphate-buffer saline
PARPs	poly(ADP-ribose)polymerases
RNF146	ring finger protein 146
SH3BP2	SH3-domain binding protein 2
S1P and S2P	site-1 and site-2 proteases
SYK	spleen tyrosine kinase
SAM	sterile alpha module
SRE	sterol response element
SREBP	sterol response element binding protein
TRF1	telomere repeat binding factor 1
TGN	trans-Golgi network
Fz	transmembrane Frizzled
WNT	Wingless-type mammary tumor virus integration site proteins
YAP	yes associated protein
β-TrCP	β-transducin repeat containing protein

Table of Contents

1 Introduction

1.1 Cancer

Cancer is defined as the result of genomic instability, where abnormal growth of any cell type leads to the development of a tumor [1]. A tumor can be benign or malignant, where a benign tumor is confined to its original location, unable to invade surrounding tissue, nor spread to distant body sites [2, 3]. However, benign tumors can still be dangerous as it can grow and compress healthy tissue. Malignant tumors are able to invade surrounding normal tissue and metastasize to distant body sites via the circulatory or lymphatic systems.

The complex development of a tumor requires many biological capabilities, which are called the hallmarks of cancer (**Figure 1**) [1]. Genetic mutations that lead to cancer are often a result of mutations in tumor suppressor genes, oncogenes or DNA repair genes [4]. Tumor suppressor genes code for inhibitors of cancer cell proliferation and survival, and mutation of these genes can prevent cells from entering apoptosis and further lead to cancer [5]. Oncogenes may develop from proto-oncogenes by mutations in ways that make the genes continuously active [6]. Oncogenes code for positive regulators of cell growth and differentiation which enhance cancerous proliferation [5, 7].

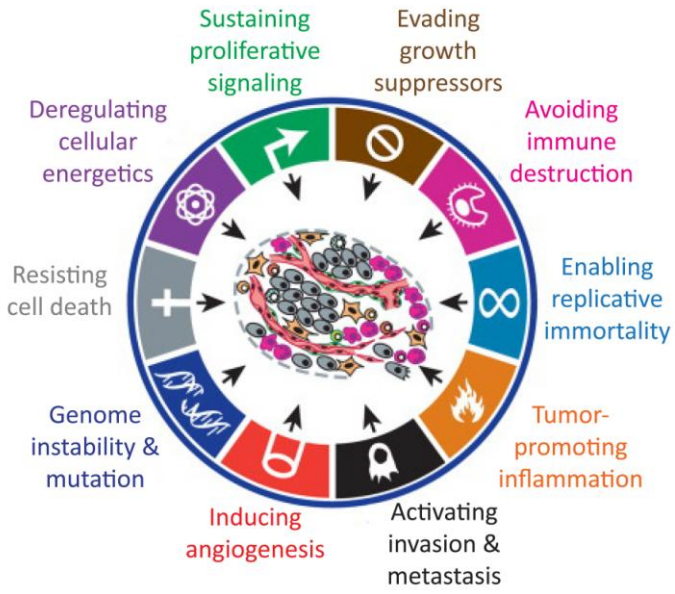

Figure 1. An overview of the hallmarks of cancer. Capabilities necessary for tumor growth and progression. Figure adapted from Hanahan and Weinberg; 2011 [1].

1.1.1 Colorectal cancer

Colorectal cancer (CRC) is defined as cancerous growth in the colon, rectum and appendix. It is the third most common form of cancer and the second leading cause of cancer-related death in the Western world [8]. There are several symptoms for CRC including change in bowl habits, diarrhea or constipation, blood in stool and a feeling that the bowl does not completely empty.

The first step in colorectal tumor development is an increased proliferation of colon epithelial cells, often as a result of mutations in the adenomatous polyposis coli tumor-suppressor gene (APC) [2, 9]. Within a proliferative population of cells, one cell often gives rise to a small benign neoplasm, adenoma or polyp. The subsequent growth of adenomas is often followed by mutations of oncogenic KRAS and the tumor suppressor SMAD4, which further increases the size and proliferation potential. The emergence of malignant carcinomas from benign adenomas, is often associated with mutations of the TP53 protein and deletions on chromosome 18q. At this stage, the tumor cells start to invade connective tissue through the basal lamina, and continue to proliferate and spread through the tissue of the colon wall. In the last stage the cancer cells succeed forcing through the wall and invade other abdominal organs, such as the bladder or small intestine. The cancer cells can also invade the blood and lymphatic systems, and through that metastasize.

Depending on the genetics and causes of disease, CRC is categorized in three types: sporadic, inherited or familial colorectal cancer [8]. The sporadic colorectal carcinoma is neither familial nor inherited disposed, and accounts for 70 % of the CRC cases. Normal aging, dietary and environmental factors are some factors which are believed to affect the risk of developing this type of CRC. About 5 % of colorectal cancer cases arise from well-defined inherited syndromes, including Lynch syndrome, Familial Adenomatous Polyposis (FAP), MYH-associated polyposis, and the rare hamartomatous polyposis syndrome [10, 11]. The remaining 25 % are familial colorectal carcinomas. This type shows commonly an increased risk among family members, without evidence for one of the known inherited syndromes, but are rather alterations in single genes that are less penetrant [8, 10, 12].

The WNT signaling pathway seem to play a crucial role in colorectal carcinoma development, were mutations in at least one WNT pathway gene is observed in over 90 % of colorectal cancer cases [13]. In more than 80 % of the cases, a loss of function mutation in the APC tumor suppressor gene is observed, creating a continued expression of the WNT

signaling pathway in the cells. Other genes that are mutated frequently in colorectal cancer are; β-catenin (*CTNNB1*), frizzled 10 (*FZD10*), T-cell factors 3 and 4 ([TCF3/4] *TCF7L1/2*), axis inhibitor 2 (*AXIN2*) and APC membrane recruitment protein 1 (*AMER1*, *WTX* or *FAM123B*).

1.2 The WNT/β-catenin signaling pathway

1.2.1 Components and regulation

The WNT/β-catenin signaling pathway is important in regulating cell fate, proliferation, survival, differentiation, migration and polarity [14]. In native cells, the WNT signaling pathway switches between an "on" and "off" state, where the amount of the transcriptional co-activator β-catenin is regulated [15]. In the off state, the signaling pathway uses a destruction complex to phosphorylate cytoplasmic β-catenin, labeling it for degradation by the proteasome. The destruction complex, is composed of the scaffolding protein AXIN1/2, APC, casein kinase 1 (CK1) and glycogen synthase kinase 3β (GSK3β). When the destruction complex captures the β-catenin, CK1 first phosphorylates β-catenin on Ser45, this enables GSK3β to sequentially phosphorylate β-catenin at Thr41, Ser37 and Ser33. This generates an ES ubiquitin ligase β-transducin repeat containing protein (β-TrCP) binding site. This phosphorylation is recognized by β-TrCP; an E3 ubiquitin ligase subunit, which induces β-catenin ubiquitination and subsequent proteasomal degradation. The constant degradation prevents β-catenin from reaching the nucleus, where it would affect the transcription of WNT targets genes. Instead, in the nuclear absence of β-catenin, Gruncho proteins repress WNT target genes and histone deacetylases (HDAC) binds to the TCF promoter.

The canonical WNT signaling pathway is activated when a WNT ligand binds to the seven-pass transmembrane Frizzled (Fz) receptor and the single-pass transmembrane proteins, low-density lipoprotein receptor protein 5/6 (LRP5/6) [14, 15]. This recruits the scaffold protein Disheveled (DVL), and leads to phosphorylation of LRP5/6 and enables recruitment of AXIN to the signalosome. When AXIN is recruited to the WNT signalosome, the destruction complex is not formed efficiently and phosphorylation of β-catenin followed by degradation is prevented. Thus, an accumulation of β-catenin in the cytoplasm occurs, which

further enters the nucleus where it acts as a co-activator for TCF to activate the WNT-target genes.

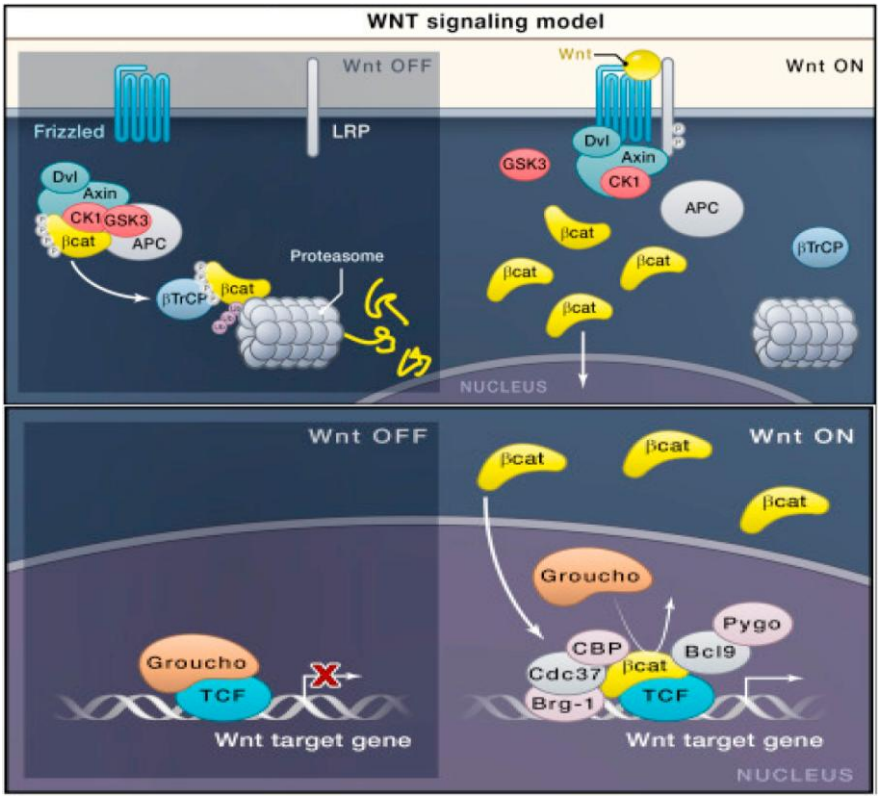

Figure 2. The WNT/β-catenin signaling pathway. The model of WNT signaling at the "off" and "on" state. The figure is modulated from Clevers and Nusse; 2012 [16].

1.2.2 WNT/β-catenin signaling as therapeutic target in cancer

The WNT/β-catenin pathway components are highly mutated in different cancers, which reflects the importance of the signaling in carcinogenesis [14]. As previous mentioned, both APC and CTNNB1 are genes that are often found mutated in colorectal carcinoma cases, creating a constitutively activated pathway, leading to tumor genesis [15]. Hence, the WNT signaling pathway may be used as a potential therapeutic target for colorectal carcinogenesis. However, the WNT signaling pathway contains only a few druggable targets [17]. One of those targets is tankyrase which was discovered as a possible target for WNT inhibition. By stabilizating AXIN and thereby the destruction complex, degradation of β-catenin is enhanced in a context dependent manner.

1.3 Tankyrase

Tankyrase 1 and 2 (Tankyrase 1/2) belong to the Diphtheria toxin-like ADP-ribosyltransferase (ARTD) enzyme super family and both are expressed in a variety of human tissues [18, 19]. This super family of enzymes are also known as poly(ADP-ribose)polymerases (PARPs) and the activity regulates diverse processes including energy metabolism and WNT/β-catenin signaling [18, 20]. The main function of this enzymes are to catalyze a post-translational modification of target proteins including tankyrase itself, using nicotinamide adenine dinucleotide (NAD+) as a co-substrate to add ADP-ribose moieties to acetyl group of substrate proteins [19, 20]. This process is called PARsylation and often marks proteins for ubiquitination and proteasomal degradation.

1.3.1 Structure

Tankyrase 1/2 share 82 % sequence identity and consist of 1327 and 1166 residues respectively [18]. Both tankyrase 1/2 contain a catalytic PARP domain at the C-terminal end. This domain is highly conserved between tankyrase 1/2, with 89 % sequence identity [18, 19]. At the N-terminal side of the PARP domain, a conserved sterile alpha module (SAM) domain is located which is implicated in the formation of either homo- or heterooligomers [18]. The bulk of tankyrase is composed of 24 ankyrin repeats arranged in five ankyrin repeat clusters (ARC) [19], which are involved in protein-protein interactions with target proteins [18]. Tankyrase 1 contains in addition a His, Pro and Ser (HPS) rich region at the N-terminal.

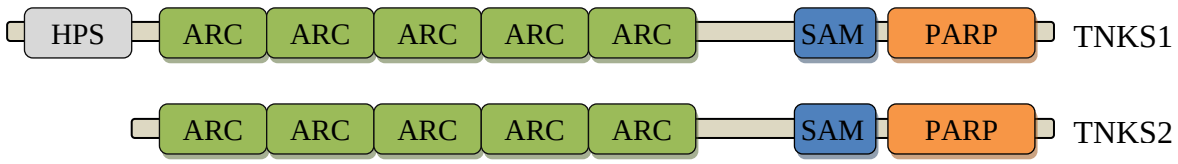

Figure 3. Domain organization of human tankyrase 1 and 2 enzymes. Both tankyrase 1 and tankyrase 2 consist of a PARP domain (catalytic domain), SAM domain (sterile alpha domain) and five ARCs (ankyrin repeat clusters). Tankyrase 1 has in addition an HPS domain (Histidine-Serine-Proline rich domain). The figure is adapted from Haikaranien, Krauss and Lehtio; 2014 [18].

1.3.2 Mechanism of action, structural and enzymatic activity

Tankyrase 1/2 excert enzymatic activity trough the catalytic PARP domain that is responsible for the ADP-ribosyltransferase activity [18]. This activity comprises the hydrolysis of NAD+ to ADP-ribose (ADPr) and nicotinamide. In the reaction the ADPr is transferred to the acceptor protein while nicotinamide is released. Amino acids on the acceptor protein known to be PARP catalyzed modified are Glu, Asp and Lys. The reaction continues by a new ADPr unit being added to the existing ADPr, which leads to a poly ADP-ribose (PAR) chain.

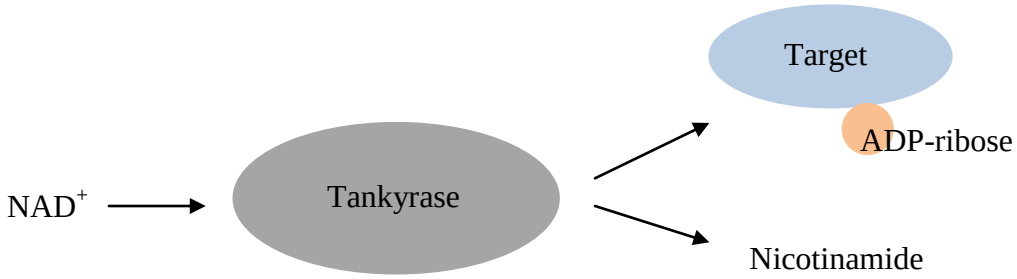

Figure 4. The PARsylation activity of tankyrase 1/2. The catalytic PARP domain of tankyrases cleaves nicotinamide adenine dinucleotide (NAD^+) to nicotinamide and ADP-ribose, where ADP-riboses are transferred to acceptor proteins and can further be recognized by secondary interacting proteins. Adapted from Jo Waaler.

Tankyrase 1/2 are also scaffolding proteins through the ankyrin repeat domain which interacts with diverse proteins [21]. The first protein to be identified as a binding partner to tankyrase was the telomere repeat binding factor 1 (TRF1) protein. Next, an insulin responsive amino peptidase (IRAP) was identified, and was shown to bind to tankyrase trough a specific six-amino acids sequence (RQSPDG). The consensus binding motif RXXPDG was further found in several bindings partner of tankyrase [22]. Peptide recognition by tankyrase requires arginine (R) at position 1 and glycine (G) at position 6, while almost any amino acid can be at position 2 and 3 [23]. Peptide position 4 favors small, hydrophobic amino acids and at position 5 aspartic acid (D) is preferred.

1.3.3 Cellular functions of Tankyrase

In mice a genetic knockout of either *Tnks* or *Tnks2* genes (encodes the proteins tankyrase 1 and tankyrase 2) generates no obvious phenotype [19]. However, mice with deficient levels of tankyrase 1 consume increased amount of food, but plasma leptin levels were decreased and the fat pad size in epididymal and perirenal was reduced [24]. It was observed that a knockout of either tankyrase genes alone did not produce an embryonic lethal phenotype, suggesting that there is high functional similarity between the two enzymes. However, inactivation of both tankyrase genes in embryos is lethal, which prove that tankyrase is an essential enzyme in embryonic development [19].

Tankyrase 1/2 has been found at multiple cellular locations, for example at the telomeres, at nuclear pores, at the Golgi complex, in the cytoplasm, at the cell membrane and at the spindle poles (**Figure 5**) [18].

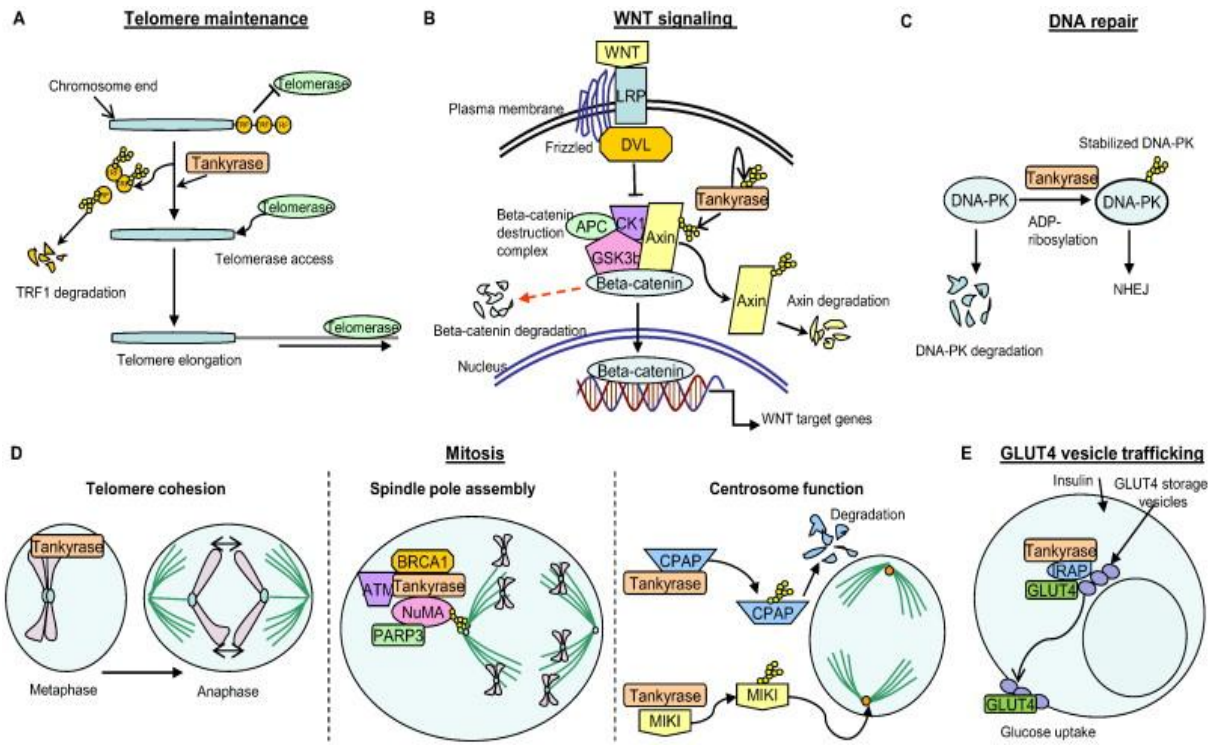

Figure 5. An overview of functions of tankyrase. A) Tankyrase PARsylates TRF1, which leads to displacement and degradation of TRF1, telomerase is able to bind the chromosome ends which leads to telomere elongation. B) PARsylation of Axin by tankyrase causes Axin degradation which further leads to disruption of the β-catenin destruction complex. As a consequence, increased amounts of β-catenin are able to move from the cytoplasm to the nucleus where they activates WNT-target genes. C) Tankyrase-mediated PARsylation of DNA-dependent protein kinase (DNA-PK), which is important in non-homologous end-joining (NHEJ) DNA repair,

leading to a release from degradation by the proteasome. D) In mitosis tankyrase has multiple roles. First, tankyrase promotes the resolution of sister chromatids at the telomeres before anaphase (left panel). Second, tankyrase forms a complex with ATM, BRCA1 and NuMA, and further PARsylates NuMA to ensure proper spindle polarity (middle panel). Finally, tankyrase interacts with CPAP and Miki which are centrosome-associated proteins, and regulates centrosome functions. E) Tankyrase regulates exocytosis of GLUT4-storage vesicles upon insulin stimulation through an interaction with IRAP. Figure from Lupo and Trusolino; 2014 [25].

1.3.3.1 Telomere maintenance

Telomeres consist of repetitive TTAGGG nucleotide sequences, which are found at both ends of each chromosome [18]. This structure protects the genome from nucleolytic degradation, recombination and interchromosomal fusion during mitosis [26]. Tankyrase 1 promotes telomeric extension by PARsylation of TRF1, which inhibits TRF1 to bind the telomeres, allowing telomerase to access it [19, 27, 28].

1.3.3.2 WNT signaling

Tankyrase 1/2 are observed to have a function in the WNT signaling pathway [19]. The scaffolding protein AXIN is the limiting component of the destruction complex [29]. When tankyrase 1/2 are active, the stability of a functional destruction complex is reduced through suppressed levels of AXIN. This leads to an increased amount of β-catenin in the cytoplasm and increased WNT signaling [18, 29]. Tankyrase PARsylates itself and AXIN, leading to recognition and binding of the E3 ubiquitin ligase ring finger protein 146 (RNF146) to the PAR tails on both proteins. The ubiquitin ligase RNF146 polyubiquitinates both tankyrase and AXIN which leads to proteasomal degradation [18].

1.3.3.3 DNA repair

DNA double-strand break (DSB) is one of the most dangerous form of DNA damage [30]. DSBs that are unrepaired cause apoptosis or senescence of cells, and mis-repaired DSBs can lead to genomic instability and carcinogenesis. Non-homologous end joining (NHEJ) is one of the most important pathways for repair of DSBs. The mechanism of NHEJ starts by recognition and rapid binding to the ends of the broken DNA molecule by Ku70/80. Ku70/80 is a scaffolding protein that recruits DNA-dependent protein kinase catalytic subunit (DNA-

PKcs) to the DNA ends and forms the active DNA-dependent protein kinase (DNA-PK) complex. It has been shown that tankyrase 1 mediates PARsylation of DNA-PKcs which is required for stabilization of the DNA-PK complex [31]. Depletion of tankyrase 1 or inhibition of its PARP activity results in degradation of DNA-PKcs which impact DNA repair functions.

1.3.3.4 Mitosis

Telomere cohesion

Sister chromatids are held together from the S phase until they are separated at mitosis by cohesin protein complexes [32]. Cohesins are removed in two steps, first from chromosome arms and second from centrosomes. Depletion of tankyrase 1 results in mitotic arrest, because the sister chromatids are still held together at their telomeres while the chromosome arms and centrosomes are separated. Telomere repeat binding factor 1 (TRF1) mediates telomere cohesion. The PARP-active tankyrase 1 is reported to dissolve telomere cohesion through ADP ribosylation of TRF1 [33].

Spindle pole assembly

When cells are at the mitotic phase (M phase), tankyrase 1 is localized to spindle poles and centrosomes where it mediates PARsylation of spindle components and is required for proper spindle polarity [18, 19]. Tankyrase 1 forms a complex with several spindle-associating proteins, which includes nuclear mitotic apparatus protein (NuMA), the protein kinase ataxia-telangiectasia mutated (ATM) and breast cancer susceptibility protein BRCA1. Tankyrase 1 function in PARsylation of NuMA, this is important in organization of microtubules at spindle pores and ensuring spindle pole bipolarity.

Centrosome function

Tankyrase regulates centrosome function by interacting with centrosome-associated proteins, such as centrosomal P4.1-associated protein (CPAP) and mitotic kinetics regulator (Miki) [25]. The centrosome is the main microtubule organization centre of the cell and consists of two centrioles which are surrounded by pericentriolar material and microtubules [34]. The duplication process of centrosomes involves formation of two procentrioles during

the S phase of the cell cycle, where CPAP is highly required. Depletion of CPAP prevents the formation of procentrioles with subsequent centrosome duplication leading to supernumerary procentrioles, centriole elongation and spindle multipolarity [34, 35]. In the early G1 phase tankyrase 1 is located at the centrosomes and PARsylates CPAP for degradation, ensuring that over-elongation of centrioles is inhibited and hence a proper function of centrosome is enabled [34]. Over expression of tankyrase 1 leads to high proteasomal degradation of CPAP, leading to an absence in centriole duplication. In contrast, depletion of tankyrase 1 stabilizes CPAP, causing elongated procentrioles and multipolarity. Tankyrase 1 PARsylation of Miki are shown to be critical for the formation of robust microtubules, that are important for proper movement of chromosomes [36].

1.3.3.5 GLUT4 vesicle trafficking

Glucose homeostasis is carefully controlled by multiple levels of regulation, where glucose transporter type 4 (GLUT4) plays a key role [37]. GLUT4 protein catalyzes hexose transport across the cell membranes through an ATP-independent, facilitative diffusion mechanism [38]. GLUT4 proteins are sequestered in intracellular membranes that are formed from either endosomes or the trans-Golgi network (TGN). These vesicles are called GLUT4 storage vesicles (GSVs) [37].

When the concentration of glucose in the blood is high, insulin secretion increases stimulating cells to take up glucose [37]. The uptake of glucose occurs by rapid translocation of GLUT4 vesicles to the cell membrane. For insulin-mediated GLUT4 translocation, motor proteins such as kinesins use microtubule networks for rapid translocation of GLUT4 storage vesicles. Tankyrase and AXIN interact with the motor protein kinesin family member 1a (KIF1a), forming an AXIN/KIF1a/tankyrase ternary complex, which is involved in an insulin dependent transport of GLUT4 vesicles from the Golgi apparatus to the cell surface to increase glucose uptake [18, 37]. In tumor cells, the level of glucose metabolism is raised, and a limiting step in exploitation of glucose is the transport of glucose through the cell membrane.

Tankyrases have also been shown to interact with the insulin-responsive aminopeptidase preotein (IRAP) [37]. IRAP is an integral membrane protein in GLUT4 vesicles, reported to play critical role in the maintenance and sorting of insulin-responsive GLUT4 vesicles.

1.3.3.6 Bone loss

A recent study has shown that inhibition of tankyrase creates decreased bone mass in mice, by increasing osteoclastogenesis [39]. It was further reported that tankyrase binds to the RSPPDG motif of SH3-domain binding protein 2 (SH3BP2). This binding represses SH3BP2 protein levels through PARsylation, which targets SH3BP2 for ubiquitination by the E3-ubiquitin ligase RNF146, followed by proteasomal degradation [39-41]. Tankyrase inhibition leads to elevated levels of SH3BP2 and increased phosphorylation of the SH3BP2-binding partner, spleen tyrosine kinase (SYK). The phosphorylated SYK controls downstream signaling leading to activation of nuclear factor of activated T cells c1 (NFATc1), which is a transcription factor for osteoclastogenesis. The Fujita and colleagues showed that tankyrase inhibition increased expression of osteoclast-associated genes. In addition tankyrase inhibitors promote osteoblast differentiation and maturation. The investigation of bone mass in mice upon tankyrase inhibition with G007-LK treatment showed that the bone volume and thickness was decreased.

1.3.3.7 Other functions

It has been shown that tankyrase inhibiton suppresses hepatocellular carcinoma cell growth via the modulation of the Hippo cascade [42]. Tankyrase inhibition is as well shown to target yes associated protein (YAP) by stabilizing the angiomotin protein family [43, 44]. Tankyrase 2 is also involved in peroxisome homeostasis and this function is independent of the enzymatic activity of tankyrase 1 [45]. A binding partner of tankyrase, tankyrase-binding protein TNKS1BP1, has been shown to regulate the actin cytoskeleton rearrangement and cancer cell invasion [46].

1.3.4 Tankyrase inhibitors

Two of the first inhibitors that showed selectivity towards tankyrase were IWR-1 and XAV939, both binds to the nicotinamide subsite in the catalytic domain [18]. XAV939, can cross react with PARP1 and PARP2 due to a high conservation of the nicotinamide subsite

between members of the PARP family [39]. Optimalization of XAV939 led to several compounds that had favorable properties [18]. Waaler and colleagues identified a new tankyrase inhibitor named JW74, which was observed to bind the adenosine subsite of the catalytic domain [47]. Optimization of JW74 by chemical analoguing led to G007-LK. This tankyrase inhibitor shows an excellent selectivity over several other isoenzymes of the PARP family, and a good activity *in vitro* and *in vivo*. Subsequently a significant number of further tankyrase inhibitors were identified [48]. In the context of WNT signaling, the tankyrase inhibition by G007-LK or other tankyrase inhibitors represses the PARsylation activity of tankyrase 1/2, leading to a stabilization of the β-catenin destruction complex component AXIN and thereby increases degradation of β-catenin [49].

1.4 Cellular cholesterol

1.4.1 Biological role of cholesterol

Cholesterol has several important roles in the cell, both as an essential structural component in the cell membrane, and as a precursor in several active molecules such as steroid hormones, bile acid, vitamin D and oxysterols (**Figure 6**) [50]. In general cancer cells tends to have increased levels of cholesterol [51] and deregulation of genes involved in cholesterol metabolism pathways have been demonstrated in colorectal cancer [52].

Cholesterol comprises of up 20-25 % of the lipid molecules in the plasma membrane, where it reduces the permeability of the plasma membrane and regulates membrane fluidity [53]. Cholesterol participates in membrane trafficking and transmembrane signaling processes through modulating the functions of membrane proteins. Cholesterol is also important in the formation of lipid rafts by acting as a spacer between the hydrocrabon chains in the plasma membrane [54]. Steroid hormones and bile acids have important roles both in signal transduction and act as solubilizers for other lipids [53]. Oxysterols are oxygenated derivates of cholesterol and the first step in the cholesterol degradation pathway [55]. Oxysterols are implied in regulating cholesterol turnover, atherosclerosis, apoptosis, necrosis, inflammation, immunosuppression and development of gallstones. The homeostasis of cholesterol is tightly regulated by uptake of cholesterol from dietary, de novo synthesis from acetyl coenzyme A (acetyl-CoA) and efflux [56].

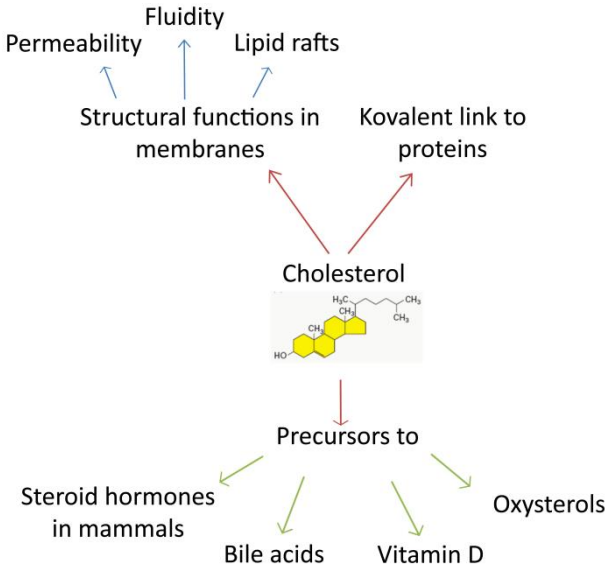

Figure 6. The functions and structure of cholesterol. Cholesterol have structural functions in the membrane, on permeability, fluidity and lipid rafts. Cholesterol is a precursor to steroid hormones, bile acids, vitamin D and oxysterols. In addition cholesterol can bind to other proteins. The figure is modified from Moore et al., 2010 [50].

1.4.2 Lipid rafts

Cholesterol can accumulate in specific regions of the plasma membrane, and combined with sphingolipids make small platforms of highly stable micro-domains called lipids rafts [57]. It has been reported that many signal transduction processes occur in lipid rafts, including processes that regulate cell survival and proliferation [58]. It has also been reported that proteins involved in the development of several malignant cancers are associated with lipid rafts, which may indicate that lipid rafts have a major role in tumor progression.

1.4.3 Cholesterol biosynthesis

The primary site of cholesterol synthesis is the endoplasmic reticulum (ER). All nucleated cells can synthesize cholesterol molecules from acetyl CoA through several enzymatic reactions, known as the mevalonate pathway (**Figure 7**) that are catalyzed by enzymes that are located in the cytosol and ER [59]. The rate-limiting enzyme of the synthesis is hydroxymethylglutaryl CoA reductase (HMG-CoAR), which catalyzes the synthesis of

mevalonate from HMG-CoA [53]. Mevalonate is further converted to squalene by a cascade of six enzymatic reactions. From squalene the first sterol, lanosterol, is catalyzed by the enzyme squalene cyclase. Lanosterol is further processed to cholesterol by a series of oxidations, reductions and demethylations [60]. There are two alternative pathways for the synthesis of cholesterol from lanosterol, the Bloch pathway and the Kandutsch-Russell pathway. Both pathways have the same enzymatic steps but differ in the step where the C24 double bond is reduced [53].

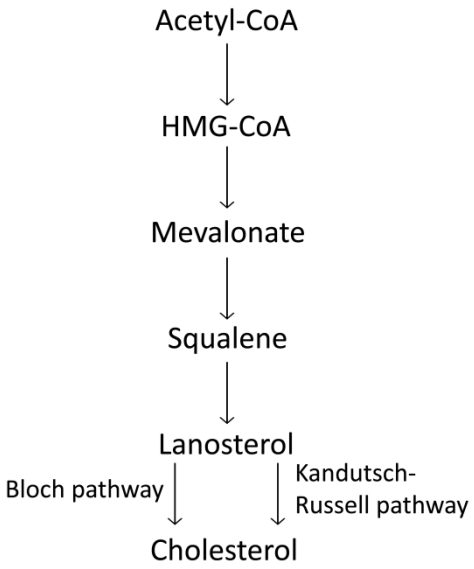

Figure 7. Overview of main steps in the cholesterol biosynthesis. Cholesterol is synthesized from acetyl-CoA through several enzymatic reactions, where the main steps are shown here. Modified from Ikonen and Elina, 2008 [53].

1.4.5 Regulation of cholesterol synthesis

The rate-limiting enzyme for the synthesis of cholesterol is HMG-CoAR [61]. When cholesterol levels are high, the intermediary product lanosterol accumulates in the ER membrane. HMG-CoAR being located in the membrane of the ER, contains a sterol-sensing membrane domain and when interacting with lanosterol the conformation of HMG-CoAR changesl. This change allows HMG-CoAR to bind to insulin-induced gene (INSIG) in the ER membrane, which is associated with proteins that lead to proteasomal degradation of HMG-CoAR.

The two main nuclear receptor systems regulating cellular cholesterol synthesis, uptake and processing are sterol regulatory element binding proteins (SREBPs) and liver X receptors (LXRs). Activation of SREBP because of low cholesterol levels increases the gene expression levels of cholesterol synthesis stimulating proteins such as HMG-CoAR and LDL receptors (LDLR) [53]. To protect the cells from cholesterol overload and removal of cholesterol from the peripheral cells, reverse cholesterol transport is stimulated by activation of LXR [53, 62]. LXR is activated by oxysterols, but this mechanism is not well understood.

A more explained mechanism for transcriptional regulation of cholesterol levels is by SREBP [53]. SREBPs in association with the SREBPs cleavage activating protein (SCAP) are located in the ER, and are kept in the ER by INSIG when the cholesterol levels are sufficient [56]. When cholesterol levels drops, SCAP dissociates from INSIG and enters COP II coated vesicles that escorts the SREBPs to the cis-Glogi. At the cis-Golgi, SREBPs are cleaved by two proteases, site-1 and site-2 proteases (S1P and S2P). This allows the N-terminus SREBP to enter the nucleus, bind to sterol regulatory element (SRE) and activate gene expression of cholesterol synthesis stimulating genes, such as genes encoding HMG-CoAR and LDL receptors. There are three isoforms of SREBP; SREBP-1a, SREBP-1c and SREBP-2, and they have different roles in lipid synthesis [63]. SREBP-2 is specific involved in cholesterol synthesis, but SREBP-1c is involved in fatty acid synthesis and insulin induced glucose metabolism. The last isomform, SREBP-1a, seems to be involved in both pathways.

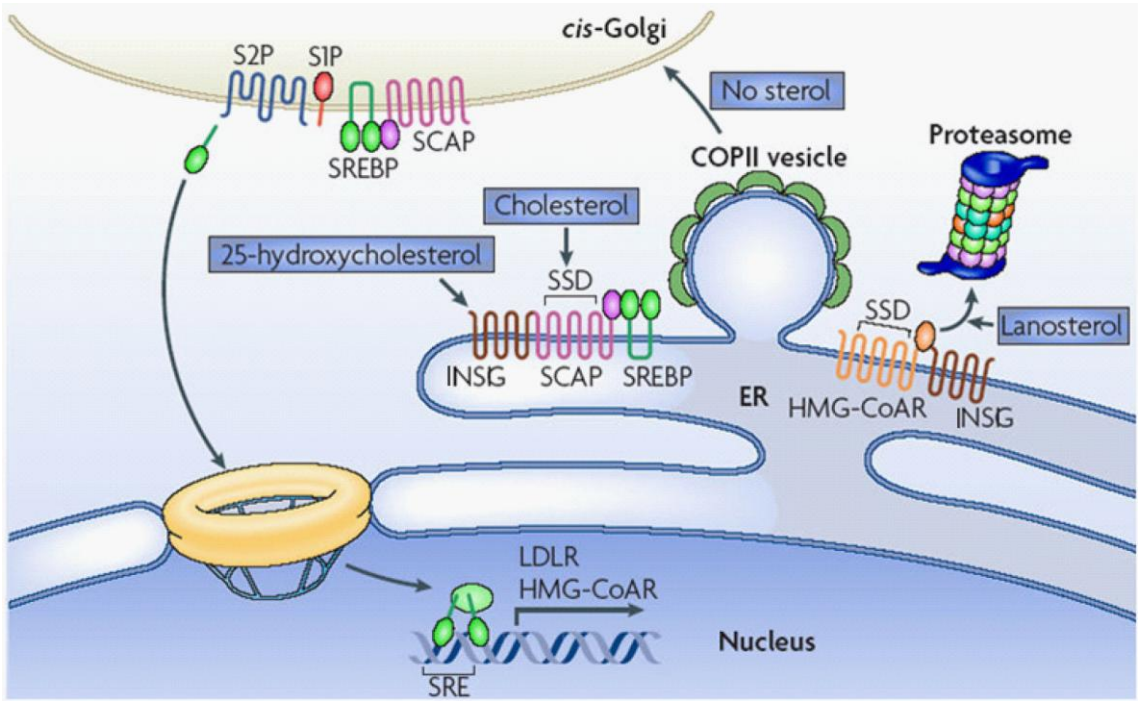

Figure 8. Overview over sterol regulatory element binding protein (SREBP) regulation of cholesterol metabolism. . When cholesterol levels are high, the protein INSIG prevents the translocation of SCAP-SREBP complex to COPII-coated vesicles. Increased cholesterol levels cause INSIG to dissociate from the SCAP-SREBP complex. This allows the complex to enter the COPII coated vesicle and transport to the Golgi. At the Golgi, SREBP are cleaved and the N-terminal is transported to the nucleus where it binds to SRE and activate sterol-regulated genes. HMG-CoAR changes conformation when interacting with lanosterols, because of increased levels of lanosterols. This change allows HMGCoAR to bind INSIG which targets is for proteasomal degrdation. The figure is from Ikonen; 2008 [53].

1.4.3 Cellular uptake of dietary cholesterol

Cholesterol that is obtained through nutrition is primarily transported from the gut to the liver, from where it is transported to other body sites [53]. For long-distance transport, through the lymph and blood stream, cholesterol is packed into lipoproteins of various size and compositions. Lipoproteins are categorized into four groups: chylomicrons, very low-density lipoprotein (VLDL), low-density lipoprotein (LDL) and high-density lipoprotein (HDL). Cholesterol derived from nutrition is first absorbed by entrocytes in the small intestine. Enterocytes package cholesterol along with triglycerides to chylomicrons [53]. Chylomicrons enter the lymphatic system and the blood stream where some of the triglycerides are hydrolyzed and new apoproteins are added to produce chylomicron remnants [64]. The chylomicron remnants are then taken up by hepatocytes and these secrete lipids and

cholesterol in VLDL particles [53]. In the blood, muscle and adipose tissue much of the triglycerides are removed and convert from VLDL to LDL, which is the main lipoprotein for cholesterol delivery to peripheral cells. Cells that have excess of cholesterol can release it to HDL and the liver can take it up and excrete the excess cholesterol into bile or repackage it for delivery to other cells.

1.4.4 Cholesterol efflux

The excess of cholesterol in peripheral tissue can be transported by high-density lipoproteins (HDL) to the liver for excretion [59]. This happens by release of cholesterol from the peripheral cells to apolipoprotein A-I (apoA-I) that is converted to HDL through lipidation. The key regulators of cellular cholesterol export are the ATP-binding cassette (ABC) transporters. The ABC transporter A1 (ABCA1) mediates the rate-limiting step in HDL particle formation [53]. The binding of free apoA-I to the ABCA1 transporters triggers a multi-step process where phospholipids and cholesterol are transferred to apoA-1 and generate pre-β-HDL. The plasma enzyme, lecithin:cholesterol acyl transferase (LCAT), esterifies cholesterol and produces globular HDL particles. These serve further as acceptors for more cholesterol that is removed from the cells by help from ABCG1, which is a second ABC transporter, and cooperates with ABCA1 by adding cellular lipids to the globular HDL resulting in the maturation of HDL.

1.4.6 The role of cholesterol metabolism in cancer

It has been shown that changes in cholesterol metabolism may have important roles in carcinogenesis and tumor development [57]. The hypothesis that cancer cells need excess of cholesterol to keep the high proliferation levels is accepted, but it is not fully understood how cancer cells reprogram cholesterol synthesis, uptake and efflux.

2 Aims of the study

The use of tankyrase inhibitors, like G007-LK, for the treatment of WNT/β-catenin driven cancers has been explored as a therapeutic strategy. However, while some cancer cell lines show reduced growth upon tankyrase inhibition, other cancer cell lines are completely resistant. In some cases the status of WNT/β-catenin signaling can show sensitivity to tankyrase inhibition, and growth reduction correlate with reduced WNT/b-catenin signaling. However, since this is rarely the case and a better understanding of cellular factors determining cells sensitivity to tankyrase inhibition is needed.

The initial goal of the work in this thesis was to use the isogenic ABC-1 wt (wild type) and ABC-1-LT (long term treated) cell lines which displayed opposite sensitivity to G007-LK treatment, as a model system to characterize factors influencing on cells sensitivity to tankyrase inhibition. The G007-LK resistant ABC-l-LT cell line had previously been established by long term propagating the G007-LK sensitive ABC-1 wt cell line in the presence of low concentrations of DMSO. The ABC-1-LT cell line was assumed to be a result of activation of adaptive mechanisms in ABC-1 WT cells due to long term DMSO treatment. However, in the first part of this thesis it was established that the ABC-1-LT cell line was unrelated to the ABC-1 wt cell line. By genetic analysis, the ABC-1-LT cell line was identified as RKO cells and it was assumed that the cells were probably selected from a contamination of the initial batch of ABC-1 wt cells with RKO cells.

Given the results in the first part of this thesis a change research focus was agreed upon. Since RKO cells were enriched due to insensitivity to tankyrase inhibition, the main goal of the second part of this work was to characterize consequences of tankyrase inhibition that neither affect WNT/β-catenin signaling nor growth. This will be accomplished by analysing previously acquired data from RNA sequencing of DMSO and G007-LK treated RKO cells to identify differentially regulated genes. Genes identified as differentially regulated upon G007-LK treatment will be used as a tool to identify and characterise cellular consequences of tankyrase inhibition.

Thus, although regulation of WNT/β-catenin signaling is the best studied consequence of tankyrase inhibition, tankyrase also impacts a number of other central cellular processes. An understanding of the plethora of consequences of tankyrase inhibition on cancer cells is an important task on the way towards developing tankyrase inhibitors in the cancer arena.

3 Materials and methods

3.1 Cell culture

3.1.1 Cell lines

The lung cancer cell line ABC-1 (JCRB Cell Bank (Japanese Collection of Research Bio resources Cell Bank), #JCRB0815) and the colon cancer cell line RKO (American type culture collection [ATCC] Cat# CRL-2577) were maintained in Eagle's Minimal Essential Medium (EMEM, #30-2003, LGC-standards) supplemented with 10 % fetal bovine serum (FBS, Life technologies, Cat#16141-079) and 1 % penicillin/streptomycin solution ([P/S], Sigma-Aldrich, Cat# P4333). The cells were cultured in a humidified chamber containing 5 % CO_2 at 37 ºC. The cell lines were routinely tested for mycoplasma infection using the MycoAlert™ Mycoplasma Detection Kit (Fischer, Cat# 11680271) according to the manufactures instructions.

3.1.2 Cell splitting

In order to keep the cells in exponential growth phase the cells where split when they reached a confluence of about 70-80 %. The split ratio for the ABC-1 cell line was 1:5 and 1:10 for the RKO cell line. The culture medium was removed and the cells were washed with phosphate-buffer saline (PBS, OUS, Ullevål, Mikroniologisk avdeling), to completely remove the remaining medium containing 10 % FBS, which inhibits the enzymatic activity of Trypsin. Subsequently, Trypsin-EDTA (Sigma-Aldrich, Cat# T3924) was added to the cells (typically 1-3 ml depending on the size of the culture flask) for about 5 minutes at 37 ºC to detach the cells from the culture flask. Cell was inspected with a microscope see when all cells had detached and then the cells were resuspended in complete culture medium and the desired amount of cells was transferred to a tissue culture flask for further propagation or used in experiments.

When plating out a specific number of cells was required, cell concentration was determined using a TC20™ automated cell counter (Bio-Rad, Hercules, California, USA)

instrument. The TC20 cell counter can count cells having a diameter from 6 to 50 μm and a concentration of $5x10^4$ – $1x10^7$ cells/ml. To count cells, 10 μl of the cell suspension was applied to the counting slide (Bio-Rad, Cat#145-0017) that was inserted into the TC20 cell counter.

3.1.3 Cell treatments

For experiments involving drug treatment the cells were plated out one day before drug containing medium was added. The following drugs and concentrations were used: CHIR (Selleck Chemicals, Cat# S2924) (dissolved in DMSO) was used at a final concentration of 2.5 μM; G007-LK (Mercachem, Cat# ME20170033a) (dissolved in DMSO) was used at a final concentration of 1 μM; for the DMSO control the amount of DMSO added was adjusted to equal the DMSO concentration used in the drug treatments. All drugs were added either to complete or lipid depleted growth medium ad indicated and the cells were incubated with the drugs for 24 hours.

For lipid depletion cells were maintained in lipid depleted medium containing 5 % Lipoprotein Deficient Serum from fetal calf ([LPDS], (Sigma-Aldrich, Cat#S5394), 10 μM Mevastatin (dissolved in EtOH) ([compactin], Sigma-Aldrich, Cat#M2537) and 50 μM Mevalonolactone (dissolved in DMSO) ([mevalonate], Sigma-Aldrich, Cat#M4667) and P/S.

3.1.4 Long-term treatment with DMSO on ABC-1 cells

To replicate previous experiments demonstrating a change in morphology and development of G007-LK resistance in ABC-1 cells after long-term exposure to 0.001 % DMSO, a new bath of ABC-1 cells was long-term treated with DMSO. Thus, ABC-1 cells were grown with and without 0.001 % DMSO added to the growth medium. The experiment was run in T25 flasks and passaged 30 times. The flasks were split in a 1:5 ratio when they reached a confluence of about 70-80 %. Medium containing DMSO was freshly prepared for each time the cells were split.

3.1.5 Plasmid purification

The pSREBP-1a (Addgene, Cat# 26801), SREBP-1c (Addgene, Cat# 26802), SREBP-2 (Addgene, Cat# 26807), pSynSRE-T-Luc (Addgene, Cat# 60444), pSynSRE-Mut-T-Luc (Addgene, Cat# 60490) and pSRE-Luciferase plasmid (ATCC, Cat#MBA-120) was delivered in transformed *Escherichia coli*. Plasmid purification was performed by growing the transformed bacteria in Luria-Bertani (LB) medium (OUS, Ullevål, Mikroniologisk avdeling) supplemented with the appropriate antibiotics on a shaker at 37 °C overnight. Next the bacterial suspension was centrifuged at 3200 G for 10 minutes. Plasmid purification from the bacteria pellet was performed using the QIAGEN Plasmid Midi Kit (Qiagen, Cat#12143) according to the manufactures instructions. Plasmid concentration was measured using a NanoDrop 2000c Spectrophotometer (Thermo Fisher Scientific).

3.2 RNA sequencing and analysis of gene expression levels in DMSO and G007-LK treated RKO cells

The results from the RNA sequencing were obtained from Jo Waaler (Krauss group) and Martin Frank Strand (Krauss lab and Kristiania University College, Oslo, Norway) who initially performed the analysis as part of a separate research project. Briefly, RKO cells were treated with 1.0 μM G007-LK and DMSO-control for 24 hours prior to total RNA extraction. RNA samples were processed and sequenced by BGI (Beijing Genomics Institute, Guangdong, China). Raw reads from the sequencing were filtered and cleaned by BGI and clean reads were mapped to reference sequences and/or reference gene set using SOAPaligner/SOAP2 [65]. No more than 2 mismatches were allowed in the alignment. Mapped reads were used to calculate gene expression level by using the RPKM (Reads Per kb per Million reads) method [66]. The RPKM values can be directly used for comparing the difference of gene expression among samples.

Differentially expressed genes (DEG's) were detected using the NOIseq method [67] and a heatmap was created using the R environment [68].

Pathway and upstream regulator analysis were performed with Qiagen's Ingenuity Pathway Analysis (IPA) software (Qiagen, Hilden, Germany).

3.3 IncuCyte live cell proliferation assay

An IncuCyte Zoom (Essen BioScience) instrument was used to measure cell proliferation rates over time. The experiment was done in 12-well plates and 35 000 cells were plated out per well, and placed at 37 °C overnight. The next day cells were incubated with 1 μM G007-LK and 0.01 % DMSO as a control and placed in the Incucyte instrment that was set to acquire phase-contrast pictures every second hour throughout the experiment. The data was analyzed by the IncuCyte Zoom software and exported to Excel for further analysis and graph design.

3.4 Western blot analysis

Western blot is an important technique in cell and molecular biology to separate and identify specific proteins from a mixture of proteins [69]. The proteins are separated according to their electrophoretic mobility that in sodium dodecyl sulfate polyacrylamide gel electrophoresis (SDS-PAGE) is determined by the proteins length and mass to charge ratio. Following separation by electrophoresis the proteins are transferred (blotted) from the PAGE gel to a polyvinylidene difluoride (PVDF) membrane where the proteins can be detected and identified by using specific primary and secondary antibodies.

3.4.1 Preparation of total cell lysates and measurement of protein concentration

For preparation of total lysates the cells in plates were lysed with 100 μl 1x Pierce® RIPA Lysis buffer (Thermo Scientific, Cat# 89901) containing Protease inhibitor Cocktail Tablets (cOmplete Tablets, Roche applied science, Cat# 4693124001) and phosphatase inhibitor Cocktail Tablets (PhosSTOP, Roche applied science, Cat# 04906837001). The cell plates with the lysis buffer were incubated 20 minutes on ice before the cell lysate were collected by using a cell scrape (Sarstedt, Cat# 83.1832) and transferred to 1.5 ml Eppendorf tubes. The lysates were then centrifuged at 13000 rpm at 4 ºC for 20 minutes, and the supernatant was transferred to new 1.5 ml Eppendorf tubes to pellet out the DNA and cell debris.

3.4.2 Electrophoresis and blotting

Cell lysates containing 20 µg total protein were mixed with NuPAGE LDS Sample Buffer (4X) (Thermo Fisher Scientific, Cat#NP0007) and heated at 70 ºC for 10 minutes and centrifuged for 30 seconds at 4000 RPM. Electrophoresis was performed using the following precast-gel and running buffer combinations: NuPAGE Tris-Acetate 3-8 % Mini gels (Life Technologies, Cat#EA0375BOX) with Tris-Acetate SDS running buffer or NuPAGE Bis-Tris 4-12 % Midi gel (Thermo Fisher Scientific, Cat#WG1402BOX) with MOPS running buffer. In each gel at least one well containing 5 µl PageRuler Prestained Protein Ladder (Thermo Fischer Scientific, Cat# 26616) was included for use as a size standard. Empty wells were filled up with diluted LDS sample buffer. The electrophoresis were first run at 60 V for 10 minutes in (order to get the samples evenly into the gel) then the voltage was changed to 150 V and the electrophoresis were allowed to run for 1 hour.

After electrophoresis the gel was removed from the plastic cassette and the stacking gel was scraped off. The gel was equilibrated in 1x Transfer buffer for 10 minutes. A piece of an Immobilon® - P^{SQ} PVDF Transfer Membrane (Merck Life Science/Millipore, Cat#ISEQ00010) was cut to the size of the gel and soaked in methanol for 20 seconds for activating, followed by equilibration in 1x Transfer buffer for 10 minutes. For semi-dry blotting the gels and PVDF membrane were placed between two thick filter papers (Bio-Rad Laboratories, Cat#1703960) that had been soaked in Transfer buffer in a Trans-Blot® SD Semi-Dry electrophoretic transfer apparatus (Bio-Rad, Hercules, California, USA) in the following (order from bottom): filter paper, PVDF membrane, gel, filter paper. After assembly a pipet was rolled over the assembly in order to remove excess transfer buffer and air bubbles. The semi-drtransfer was performed for 60 minutes at 25 V (300 mA).

Table 1. 10x Transfer buffer

Components	
Trizma-base (Sigma-Aldrich, Cat#T1503)	30.3 g
Glycine (Sigma-Aldrich, Cat# G7126)	144.0 g
MQ H_2O	To 1000 ml

Table 2. 1x Transfer buffer

Components	
10x Transfer buffer	100 ml
MeOH (VWR, Cat#20903.368)	200 ml
MQ H_2O	To 1000 ml

3.4.3 Antibody incubation and protein detection

Following protein transfer, the PVDF membrane was blocked with a solution of 5 % Nonfat milk (AppliChem, Cat#A0830.0500) in TBST (Tris Buffered Saline with Tween (prepared from tablets (Medicago, Cat#09-7510-100) dissolved in distillated H_2O) for 1 hour at room temperature. Next, the PVDF membranes were incubated with the appropriate primary antibodies (diluted in 5 % milk in TBST) overnight at 4 ºC. After washing 3x10 minutes with TBST the membranes were incubated with horseradish peroxidase (HRP) conjugated secondary antibodies in 5 % milk, TBST for 1 hour at room temperature. All primary and secondary antibodies and dilutions used in this study are listed in table 3. Before chemiluminiscent detection the membrane were washed 3x10 minutes in TBST before the ECL-Prime detection reagent was added for 5 minutes at room temperature according to the manufactures instructions. Detection of chemiluminiscent signals and image acquisition was done using the ChemiDoc^{TM} Touch Imaging System (BIO-RAD).

Table 3. Antibodies and dilutions used in WB.

Target protein	Host species Ab produced in	Dilution (in 5 % milk)	Manufacture	Catalogue number
Primary antibodies				
β-catenin	Mouse	1:2000	BD biosciences	610154
Actin	Rabbit	1:4000	Sigma-Aldrich	A2066
SREBP-1	Mouse	1:100	Santa Cruz biotechnology	Sc-17755
SREBP-2	Mouse	1:100	Santa Cruz biotechnology	Sc-27161
SREBP-2	Rabbit	1:200	Abcam	Ab30682
ANTI-FLAG® M2	Mouse	1:1000	Sigma-Aldrich	F1804
Secondary antibodies				
Anti-mouse IgG HRP	Chicken	1:5000	Santa Cruz biotechnology	#K1113
Anti-rabbit IgG HRP	Chicken	1:5000	Santa Cruz biotechnology	#K2514

3.5 Immunofluorescent staining of cells

Immunofluorescent staining (IF) is a method for labelling proteins in fixed cells by using specific primary antibodies that binds to the protein of interest [70]. The subcellular localization of the labelled proteins can be then be studied by fluorescent microscopy. In direct IF the primary antibody is directly conjugated to a fluorescent label, while in indirect IF detection of the primary antibody is done by using a fluorescently labelled secondary antibody that binds to the primary antibody. Fluorescent labelling of cell structures can also be performed by using various fluorescently labelled probes that has affinity for the structure of interest. In this work both indirect IF and fluorescently labelled probes was used.

3.5.1 Poly-L-lysine coating of cover glasses for IF

In order to perform high resolution fluorescence microscopy cells had to be grown on 1.5 high precision cover glasses before IF staining. In order to facilitate cell attachment the cover glasses were coated with Poly-L-Lysine before the cells were added. For Poly-L-Lysine coating, 18 mm round, cover glass (VWR, Cat# MARI0117580) were placed in 12 well plates and 1 ml Poly-L-lysine solution (SCBT, Cat#sc-286689) was added to each well. After 5 minutes incubation in room temperature the Poly-L-lysine was then removed and the cover glasses were washed two times in PBS and air dried for at least 2 hours. Sterilization after coating was performed by placing the 12 plate containing cover glasses under a UV-light source for 20 minutes.

3.5.2 Immunostaining of cells

Cells grown of cover glasses were washed with cold PBS and fixed with 350 µl ice cold 4 % paraformaldehyde ([PFA], Sigma Aldrich, Cat# 158127) in PBS for 15 minutes at room temperature (RT). The cells were then washed two times with PBS and permeabilized with 400 µl 0.1 % Triton X-100 (Roche Diagnostics, Cat# 10789704001) in PBS for 15 minutes in RT. Next the 400 µl 4 % BSA (Saveen & Werner, Cat# B2000) in PBS was added to the cells for 15 minutes in order to block unspecific antibody binding. Primary antibodies were diluted in 4 % BSA/PBS and added to the cells either for 1 hour at RT or overnight at 4 ºC. The primary antibodies and dilutions used are shown in Table 4. Next the cells were washed three times with PBS before secondary antibody diluted in 4 % BSA/PBS was added to the cells for one hour at RT. The secondary antibodies and dilutions used are shown in Table 4. For labeling of indicated cellular organelles or structures (actin filaments, golgi or lipid rafts) the appropriate fluorescent marker was added and incubated along with the secondary Ab as indicated in Table 5. Mitochondrial staining was performed by incubating the cells for 30 minutes with Mitotracker-Red (Table 5) before fixation and immunostaining. After staining the cells were then washed three times with PBS followed by nuclear counter staining by incubation with DAPI (Sigma Aldrich, Cat# D9542) (1 µg/ml) for 5 minutes at RT. The cover glasses was then mounted to a microscope slides (VWR, Cat#631-9461) using ProLong™ Diamond Antifade Mountant (Thermo Fisher Scientific, Cat#P36961). The slides were allowed to dry overnight at RT in the dark and then stored at 4 ºC until microscopy.

Table 4. Antibodies and dilutions used in IF.

Target protein	Host species Ab produced in	Dilution	Manufacture	Catalogue number
PRIMARY ANTIBODIES				
β-catenin	Mouse	1:500	BD biosciences	610154
TNKS	Mouse	1:50	Santa cruz biotchnology	sc-365897
Anti-GM130	Rabbit	1:50	abcam	ab52649
SECONDARY ANTIBODIES				
Anti mouse-Alexa-Fluor-488	Mouse	1:500	Thermo Fisher Scientific	a28175
Anti mouse-Alexa-Fluor-647	Mouse	1:500	Thermo Fisher Scientific	a31571
Anti rabbit-Alexa-Fluor-594	Rabbit	1:500	Thermo Fisher Scientific	a11012
Anti rabbit-Alexa-Fluor-568	Rabbit	1:500	Thermo Fisher Scientific	a10042

Table 5. Fluorescent markers used in IF for labeling of cell organelles and structures.

Probe name	Organelle labelled	Concentration	Manufacture	Catalogue number
Phalloidin-Alexa-Fluor-488	Binds to F-actin. Used as marker for actin filaments.	0.1 μM (together with secondary Ab)	Thermo Fisher Scientific	A12379
Lectin HPA-Alexa-Fluor-647	Binds to terminal α-N-acetylgalactosaminyl residues. Used as marker for the Golgi.	0.1 μg/ml (together with secondary Ab)	Thermo Fisher Scientific	L32454
Cholera Toxin B Subunit-FITC	Bins to ganglioside GM1. Used as a marker of membrane lipid rafts.	10 μg/ml (together with secondary Ab)	Sigma Aldrich	C1655
MitoTracker-Red-CMXRos	Stains mitochondria	50 nM (on cell for 30 minutes before fixation)	Thermo Fisher Scientific	M7512

3.5.3 Microscopy

Fluorescent images were acquired with a Zeiss Elyra PS1 microscope system using standard filters sets and laser lines with a Plan-APOCHROMAT 63x 1.4 NA oil objective. Images were acquired using the Laser wide field (WF) or Structured Illumination Microscopy (SIM) mode of the system as indicated. Laser WF images were acquired for 30 Z planes with a Z spacing of 0.08 nm between planes. Laser WF images are displayed as maximum intensity projections rendered from all Z planes. SIM is a super resolution light microscopy technique that can provide images with a twofold improvement in the resolution to Laser WF [71]. SIM images were acquired using 5 grid rotations with the 0.51μm grid for 30 Z planes with a Z spacing of 0.184 nm between planes. SIM images were reconstructed with the following "Method" parameters in the ZEN black software (Carl Zeiss MicroImaging): Processing: manual; Noise Filter: -5.5; SR Frequency Weighting: 1; Baseline Cut; Sectioning: 100/83/83; Output: SR-SIM; PSF: Theoretical. All SIM images are displayed as maximum intensity projections rendered from all Z planes.

3.5.4 Filipin fluorescence staining of free cholesterol in cultured cells

Filipin III is a naturally fluorescent polyene antibiotic which binds free cholesterol [72]. Filipin III (Sigma-Aldrich, Cat#F4767) was dissolved in DMSO to obtain a stock solution of 10 mg/ml. A working solution was prepared by diluting the Filipin III stock solution in PBS containing 10 % FBS to a final concentration of 0.05 mg/ml. For cholesterol staining cells were washed three times with PBS and fixed with 4 % PFA for 15 minutes at RT. The cells were then washed three times before staining in 350 μl Filipin working solution for 45 minutes at RT. The cells were washed three times with PBS before imaging using the DAPI filter settings on the microscope. Given that Filipin staining photobleaches very quickly imaging was performed immediately after staining.

3.6 Flow cytometric quantification of filipin staining

Cells were plated out in 6 wells plates (500 000 cells/well) and treated with 1.0 µM G007-LK for 24 hours before wash in PBS followed by addition of 400 µl trypsin per well. The cells were then resuspended in 1 ml EMEM and centrifuged at 2000 rpm for 3 minutes. The cells were washed with PBS and resuspended in 500 µl 4 % PFA (in PBS) and incubated for 15 minutes at room temperature. Next, the cells were washed again in PBS before resuspension in 500 µl Filipin working solution and incubation for 45 minutes at room temperature. Lastly the cells were washed once in PBS before resuspension in 1 ml PBS. Flow cytometric quantification was immediately performed on a Partec PAS flow cytometer using the HBO lamp for UV excitation and the DAPI filter set. For each sample 20 000 cells was acquired.

3.7 Plasmid transfection using FuGENE HD

Transfection was performed in 6-well plates and the day before transfection 450 000 cells was plated out per well. The transfection was performed according to the manufactures recommendations using µg of DNA and µl of Fugene HD per well as shown in **Table 6** and **Table 7**. At the day of transfection the medium was removed and 2 ml medium without P/S was added. Plasmid DNA was diluted in 150 µl Opti-MEM (Invitrogen, Cat# 31985-047) before addition FuGENE HD (Nerlien Mezansky, Cat#E2311) and incubation for 10 minutes at RT. Next, the transfection mixture was added to the cells and incubated over night at 37 °C and 5 % CO_2.

Table 6. **Plasmids transfected into cells for western blot analysis.**

Plasmid/pr well in a 6 wells plate	Concentration	Fugene HD
pcDNA3.1	4 µg	12 µl
pSREBP-1a	4 µg	12 µl
pSREBP-1c	4 µg	12 µl
pSREBP-2	4 µg	12 µl

Table 7. Plasmid mix transfected into cells for reporter gene assay.

Plasmid/well in a 6 wells plate	Concentration
Reporter construct one	**8,4 µg DNA + 25,2 µl Fugene HD**
pRL (Renilla Luciferace)	0.4 µg
pSynSRE-Mut-T-Luc	3 µg
pSynSRE-T-Luc	3 µg
pEGFP, pSREBP-1a, pSREBP-1c or pSREBP-2	2 µg
Reporter construct two	**5,2 µg DNA + 15,6 µl Fugene HD**
pRL (Renilla Luciferace)	0.2 µg
pSRE-Luciferase	3 µg
pcDNA3.1, pSREBP-1a, pSREBP-1c or pSREBP-2	2 µg

3.8 Dual-Luciferase Reporter Assay

The Dual-Luciferase Reporter Assay System (Promega Nerliens, Cat# E1980) was used to measure the activity of both the firefly and the Renilla luciferase reporter genes sequentially in the same sample. Reporter gene assays are used to study signalling pathway activity, gene regulation and the structure of regulatory elements. Generally a reporter gene construct consists of a regulatory element of interest driving the expression of a reporter gene that can conveniently quantified. In this thesis the reporter gene constructs used contained the sterol regulatory element (SRE) controlling the expression firefly luciferase reporter gene. If the activity of the SRE promoter is increased, the cells will make more of the firefly luciferase protein. A constitutive active Renilla luciferase construct was co-transfected with the firefly luciferase reporter gene construct in order to normalize against variability due to variations in factors including: transfection efficacy, cell numbers, cell viability, pipetting accuracy and cell lysis efficiency.

For the reporter gene assays cells were transfected in 6 well plates with the reporter gene constructs as described in section 3.7. The day after transfection the cells were trypsinized, counted and 20 000 cells were seeded pr well in 96 well plates (Perkin Elmer, Cat# PER 6005680) and added treatment the day after. The cells were then treated with G007-LK for 24 hours before lysis; The growth medium was removed and the cells were washed with PBS.

After PBS removal, 40 µl of 1x Passive Lysis Buffer (PLB) was added to each well. The culture plate was placed on a shacker for 20 minutes at RT. The lysates were either placed at -800C for storage or analyzed directly.

The Dual-Luciferase Assay was performed according to the manufactures recommendations and the assays reagent was prepared as following: LARII was prepared by resuspending the lyophilized Luciferase Assay Substrate in 105 ml of Luciferase Assay Buffer II. The Stop & Glo reagent was prepared by adding 1 volume 50 X Stop & Glo® Substrate to 50 volumes of Stop & Glo Buffer. For luciferase measurement 10 µl of cell lysate (in PLB) was transferred to a new 96-well plate that was placed in the GloMax Microplate Luminometer (Promega). Injectors 1 and 2 were set to dispense 50 µl of LAR II and Stop & Glo Reagent. The luminometer was programmed to use a 2 seconds delay and 5-10 seconds read time. Thus, the luminometer first dispenses 50 µl LARII (pr well) followed by quantification of firefly luminescence. The firefly reaction in quenched by addition of 50 µl of Stop & Glo Reagent (pr well) that also initiate the Renilla luciferase reaction so Renilla luminescence can be quantified. A normalized value for SRE-Luciferase repoter gene activity was calculated by dividing the values for firefly luminicence with the values for Renilla luminescence. For each treatment at least 4 parallels were included.

3.9 Real-Time quantitative polymerase chain reaction analysis (RT-qPCR)

Total RNA was isolated using the GenElute Mammalian Total RNA Purification Kit (Sigma-Aldrich, Cat #RTN350) according to the supplied protocol. The SuperScript VILO cDNA Synthesis Kit (Life Technologies, Cat #4309849) was used to synthesize cDNA from 2 µg of RNA as template. Selected TaqMan probes were diluted 1:1, and a mix containing 5 µl TaqMan Gene Expression Master Mix (Life Technologies, Cat #4309849), 3µl MQ water and 1 µl cDNA for each well was made. To each well of a MicroAmp Optical 384-Well Reaction Plate with Barcode (Life Technologies, Cat #4370074) 1 µl probe and 9 µl of the mix was added with 3 replicates. In this thesis, the following TaqMan probes were used: *GAPDH* (ID#Hs02758991_gl) as a endogenous reference gene, *MSMO1* (Thermo Fisher Scientific, Cat# Hs00932159), *DHCR7* (Thermo Fisher Scientific, Cat# Hs01023087), *INSIG1* (Thermo Fisher Scientific, Cat# Hs00356479), *CYP51A1* (Thermo Fisher Scientific, Cat# Hs01567880)

and *SREBP-1c* (Thermo Fisher Scientific, Cat# Hs01088691). After addition of all components the 396 well plate was sealed with MicroAmp Optical Adhesive Film (Life technologies, Cat #4311971) before the plate was centrifuged. The RT-qPCR assay was performed on a ViiA™ Real-Time PCR System (Life Technologies, Cat #4370074).

3.10 Quantification of oxysterol levels

Trypsinized cells were washed in PBS, counted and 300 000 cells were transferred to Eppendorf tubes (Protein LoBind Tubes, Eppendorf cat.nr: 022431081). After centrifugation and removal of the supernatant the cell pellet was lysed in 300 µl EtOH containing 400 nM C13 labeled "heavy" cholesterol.

Quantification of oxysterol levels was performed at the Department of Chemistry, University of Oslo by Hanne Røberg-Larsen. Briefly, Oxysterols were derivatized into Girard T derivates as described by Roberg-Larsen *et. al* [73], with some modifications: internal standard mixture consisted of 24S-hydroxycholesterol-d7, 22R-hydroxycholesterol-d7, 25-hydroxycholesterol-d6 and 27-hydroxcholesterol-d6, all from Avanti Polar Lipids inc, Alabaster, AL, USA. Final concentration of internal standard was 200 pM. Samples and calibration solutions were analyzed using a Dionex Ultimate 3000 pump coupled to a vantage triple quadrupole mass spectrometry (Both Thermo Scientific, Waltham, MA, USA) equipped with an waters 10-port valve controlled by the pump. AFFL-SPE set up was as described by Roberg-Larsen *et. al* [74]. Loading mobile phase flow was 150 µL /min and injection volume was 100 µL. Loading time was 2 minutes. Mobile phase A was 0.1 % formic acid in type 1 water (Millipore) and mobile phase B was 0.1 % formic acid in methanol. Column temperature was 30 °C and flow 50 µL/min. Separation was achieved on a 1 mm ID x 100 mm ACE 3 C18 column (Advanced chromatography technologies LTD, Aberdeen, Scotland) using a mobile phase gradient from 75 % B to 95 % B in 15 minutes, holding 95 % B for 10 minutes followed by a recondition step at 75 % B for 5 minutes. The MS was operated in SRM mode monitoring *m/z* 514.4→455.4 and 427.4 (oxysterols), *m/z* 520.4 →461.4 and 433.4 (d6-internal standards) and *m/z* 521.4 →462.4 and 434.4 (d7 internal standards).

3.11 Statistics

All statistical analysis was performed by a Student`s unpaired *t* test, were the two-tailed p value was calculated and was counted as statistically significant when p value < 0.05. To calculate the p value and statistically significant a webpage named Quick Calcs was used [75].

4 Results

4.1

Part I: Identifying a RKO cell line contamination in G007-LK resistant long term DMSO treated ABC-1 cells.

4.1.1 Characterization of wild type ABC-1 versus long term DMSO treated ABC-1 cell line.

It has been established previously that not all cancer cell lines are sensitive to growth inhibition by G007-LK treatment [29] and the initial goal of the work in this Thesis was to use the ABC-1 wild type (wt) and the long term DMSO treated ABC-1 cells (termed ABC-1 LT cells from now) as tools for characterizing the molecular mechanisms determining cells sensitivity to G007-LK treatment.

The lung cancer derived ABC-1 cell line is sensitive to tankyrase inhibition and G007-LK treatment of ABC-1 cells results in significant growth reduction (Waaler *et al.* Manus in preparation). Interestingly previous work in the Krauss lab has indicated that long term treatment of ABC-1 cells with low concentrations of DMSO, which is used as the solvent for G007-LK, led to adaptive responses making the ABC-1 cell resistant to G007-LK treatment. It was further shown that the ABC-1 LT had changed morphology from a tightly packed epithelial to an elongated fibroblast like phenotype and that the ABC-1-LT cells displayed increased proliferation rates. To characterize the previously established ABC-1 wt and ABC-1-LT cell lines we initially quantified their sensitivity to G007-LK treatment. As seen in **Figure 9A** treatment ABC-1 wt and ABC-1-LT cell lines with 1 μM G007-LK resulted in a 25 % growth reduction in the ABC-1 cell line, while the ABC-1-LT cell line displayed no change in proliferation rates upon G007-LK treatment for 60 hours. An important function of tankyrase is to regulate the levels of WNT/β-catenin signaling activity this by modifying the activity of the destruction complex through regulating AXIN levels. To investigate potential differences in β-catenin localization and protein levels, immunofluorescence (IF) and western blot analysis of β-catenin was next carried out. As seen in **Figure 9B** Western blot analysis revealed that ABC-1 cells expressed β-catenin while in ABC-1-LT no β-catenin protein could

be detected. To investigate whether the lack of β-catenin in ABC-1-LT cells was due to a genetic change or if β-catenin expression could be rescued/induced we next treated the cells with CHIR which is a specific inhibitor of GSK3β [76]. CHIR treatment did not influence on the β-catenin protein levels in ABC-1 cells, however in ABC-1-LT cells GSK3β inhibition led to increased amount of β-catenin protein reaching level similar to what was observed in untreated ABC-1 cells (**Figure 9B**). IF analysis showed that β-catenin was mainly localized at the membrane in ABC-1 cells and in agreement with the western blot analysis no β-catenin could be detected in ABC-1-LT cells (**Figure 9C**). CHIR treatment of ABC-1 cells did not alter the localization of β-catenin in ABC-1 cells while in ABC-1-LT cells CHIR treatment led to induction of β-catenin that was mainly localized at the cytoplasm. Another feature reported for the ABC-1-LT cell line was the change of morphology to an elongated fibroblastic phenotype with increased pseudopodia [77]. To characterize the actin filaments in ABC-1 and ABC-1-LT cells IF staining of filamentous (F) actin by phalloidin was carried out. As seen in **Figure 9D** there was a striking difference in F-actin staining pattern where ABC-1 cells displayed thin mostly intracellular F-actin filaments and ABC-1-LT cells contained long thick F-actin filaments protruding from the cells in filopodia like structures.

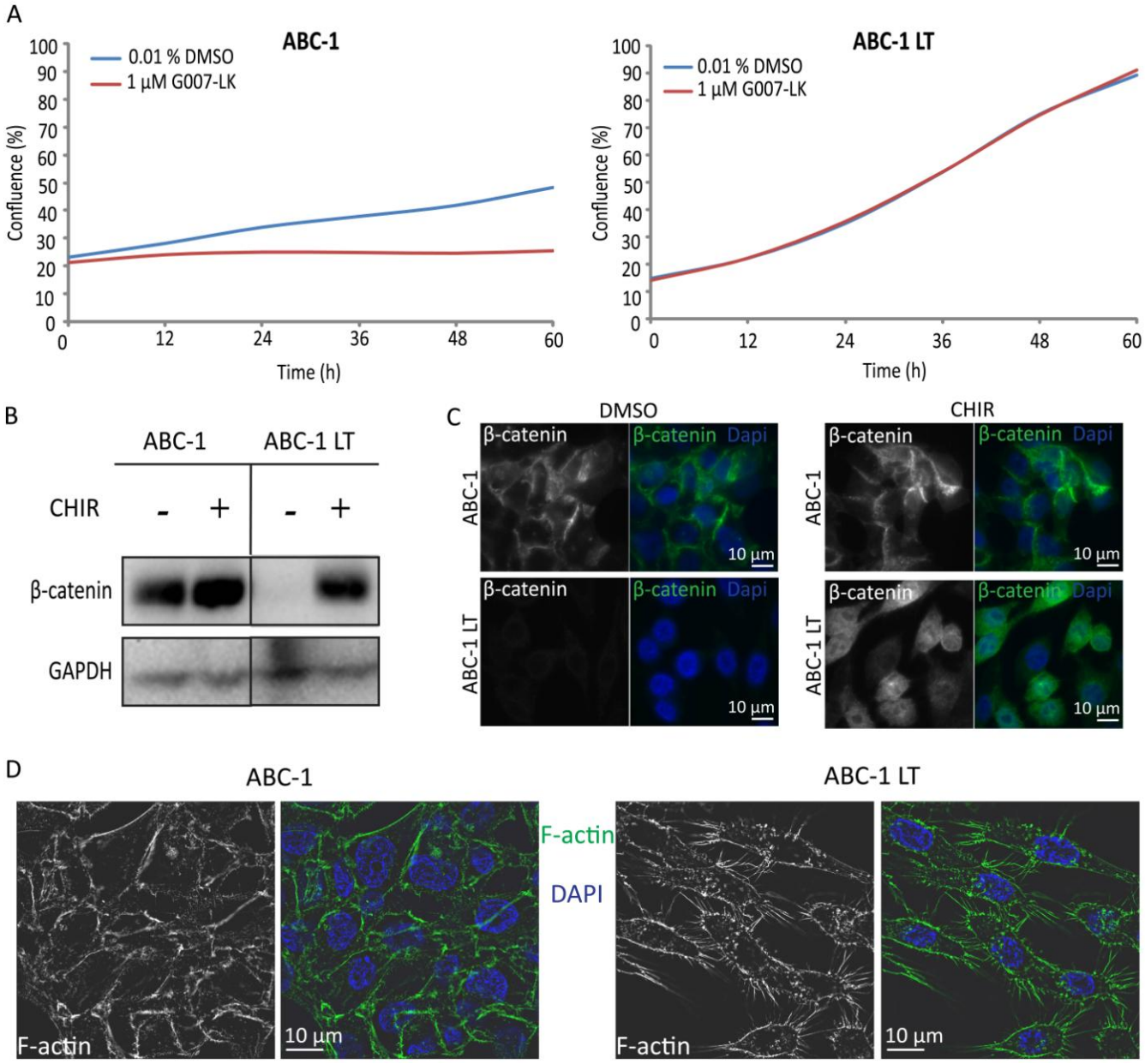

Figure 9. Characterization on ABC-1 and ABC-1 LT cells sensitivity to G007-LK treatment and analysis of β-catenin expression levels and subcellular localization.

A) Representative growth curves of ABC-1 and ABC-1-LT cells growing in the presence of DMSO (blue) or G007-LK (red) as indicated.

B) Western blot analysis of β-catenin protein levels in ABC-1 and ABC-1-LT treated with CHIR (2.5 µM) for 24 hours as indicated.

C) Representative images of ABC-1 and ABC-1 LT cells grown in the presence of DMSO (0.01 %) or CHIR (2.5 µM) for 24 hours before fixation and IF staining for β-catenin as indicated. DAPI was used for nuclear staining.

D) IF staining of actin filaments in ABC-1 and ABC-1-LT cells as indicated. The image shown was acquired by Structured illumination microscopy (SIM).

4.1.2 Failure to reproduce generation of ABC-1-LT cells by long term DMSO treatment of ABC-1 cells and detection of cross contamination of ABC-1 cell line with RKO cells.

In the previous work at the Krauss lab the generation of ABC-1-LT cells by long term DMSO treatment of ABC-1 cells had been repeated in three independent experiments. Interestingly, in all three replications a characteristic morphological change from a tightly packed epithelial to a more elongated fibroblast-like phenotype of the ABC-1 cells occurred around passage eight after first exposure to DMSO [77]. Given that in the previous study the initial aim was to study G007-LK versus DMSO treated ABC-1 cells a side-by-side control of untreated ABC-1 cells was not included. Therefore, initially in this work we wanted to generate a new ABC-1-LT cell line and in parallel also propagate untreated ABC-1 cells as a negative control. Accordingly a fresh batch of ABC-1 cell was ordered from the supplier and grown with and without 0.001 % DMSO added to the growth medium. Both the untreated and DMSO treated ABC-1 cells were splitted regularly as described in the materials and methods. Before trypsination the cells were inspected by microscopy for detection of the characteristic morphological change that was previously reported to occur around passage eight in the DMSO treated cells. As seen in **Figure 10** propagation of the new batch of ABC-1 cells in the presence of 0.001 % DMSO for 30 passages did not induce the reported change in morphology and both the untreated and the DMSO treated cells displayed a tightly packed epithelial morphology that is normal for ABC-1 cells. The attempt to create ABC-1-LT cells by long term DMSO treatment of ABC-1 cells was repeated two independent times, however in neither of the experiments the previously reported change in morphology was observed.

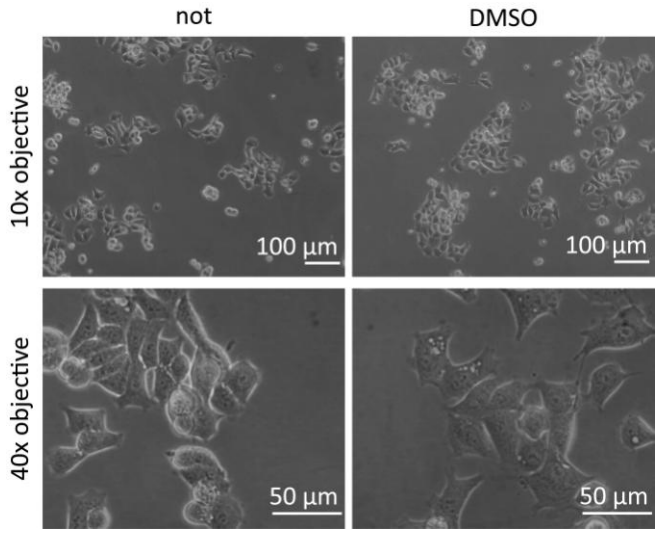

Figure 10. Morphology of ABC-1 cells propagated for 30 passages

Representative pictures of ABC-1 cells without or in the presence of 0.001% DMSO after 30 passages. Shown are images acquired at 2 different magnifications as indicated.

Given that the generation of ABC-l-LT cells had successfully been repeated three independent times from starting from the old batch of ABC-1 cells and could not be reproduced when using a new batch of ABC-1 cells led us to perform cell line identification by Short Tandem Repeat (STR) analysis. STRs are repeated segments of DNA that are typically 2-6 base pairs in length and one inherits one allele from each parent. These STRs are scattered throughout our genome. The number of repeats of each STR at each genetic site varies within cell lines, and this variability in the number of repeats makes STR DNA testing extremely valuable as a cell line identification tool. Studies have shown that in addition to the amelogenin (AMEL) the sex determination marker, a minimum of eight core STR markers are recommended to positively identify human cell lines [78]. To do the STR analysis genomic DNA was isolated from the old and new batches of the ABC-1 cell line together with the previously established ABC-1-LT cell line. The genomic DNA was submitted to Eurofins Genomics that performed the STR analysis. As seen in **Table 8** the analysis of 21 genetic STR markers showed that the old and new batch of ABC-1 cells contained identical STR pattern, in contrast the ABC-1-LT cell line diverged from the ABC-1 cells at all STR loci except from the AM loci that is used for sex typing.

Table 8. STR profiles of ABC-1 and ABC-1 LT cell lines. Length of the analyzed STR loci for each cell line is shown as indicated. For the ABC-1-LT cell line numbers in red indicates STR lengths that diverge from the ABC-1 cell lines.

STR locus	ABC-1 old batch	ABC-1 new batch	ABC-1 LT
AM	X, X	X, X	X, X
D3S1358	15, 15	15, 15	16, **19**
D1S1656	16, 18.3	16, 18.3	**14**, **17.3**
D6S1043	18, 18	18, 18	**13.1**, **19**
D13S317	8, 8	8, 8	8, **11**
Penta E	5, 16	5, 16	**11**, **13**
D16S539	9, 12	9, 12	**13**, **13**
D18S51	18, 18	18, 18	**11**, **12**
D2S1338	19, 24	19, 24	**16**, **16**
CSF1PO	12, 12	12, 12	**8**, **10**
Penta D	8, 11	8, 11	**10**, 11
TH01	10, 10	10, 10	**6**, 10
vWA	16, 16	16, 16	16, **22**, **23**
D21S11	30, 32.2	30, 32.2	**27**, 30
D7S820	10, 12	10, 12	**8**, 10
D5S818	12, 12	12, 12	**11**, **13**
TPOX	8, 11	8, 11	**11**, 11
D8S1179	13, 14	13, 14	**9**, 13, 14
D12S391	20, 20	20, 20	**15**, 20
D19S433	13, 13	13, 13	**14**, **14**
FGA	22, 22	22, 22	**20**, **21**, **23**

Cell line identification was performed by comparing results from eight STR loci with STR profiles from other cell lines using the online database at DSMZ (Deutsche Sammlung von Mikroorganismen und Zellkulturen). In the DSMZ the identity of two cell lines (A and B) is expressed as an evaluation value (EV) calculated as EV = (Number of coincident peaks of STR profiles between A and B) x 2 / (Total number of peaks of STR profiles in A and B) and

EV values greater than 0.9 indicate that the two cell types are derived from the same origin. As seen in **Table 9** the ABC-1 cell line had a complete match with the STR profile for ABC-1 cells in the DSMZ database with an EV of 1. When the DSMZ cell line database was search against with the STR profile obtained for the ABC-1-LT cell line the closest matching identified cell line was the p53R (JUH-56) cell line with an EV value of 0.92. The second and third best matches were the RKO and the RKO-AS45-1 cell lines with EV values of 0.84 and 0.77 respectively. Interestingly the p53R cell line has been discontinued from sale by ATCC (American Type Culture Collection) due to misidentification and it has been shown that the p53R cell line was derived from RKO cells [79].

Table 9. STR cell line identification of the ABC-1 cell line. STR analysis of the ABC-1 cell line using the online DSMZ database. The evaluation value (EV) was calculated as EV = (number of generated peaks cell line A) x 2 (total number of peaks of cell line A + B). EV values greater than 0.9 indicate that the two cell types are derived from the same origin. The table shows cell lines identified with an EV > 0.7 relative to the ABC-1 cell line. Numbers in red indicates STR lengths that diverge from the ABC-1 cell line.

			STR locus								
			AM	**D5S818**	**D13S317**	**D7S820**	**D16S539**	**vWA**	**TH01**	**TPOX**	**CSF1PO**
Evaluation Value	**Cell line No.**	Query: **ABC-1**	*X,X*	*12,12*	*8,8*	*10,12*	*9,12*	*16,16*	*10,10*	*8,11*	*12,12*
1.00(36/36)	JCRB0815	ABC-1	X,X	12,12	8,8	10,12	9,12	16,16	10,10	8,11	12,12
0.72(26/36)	RCB2640	G-415	X,X	12,12	8,10	11,12	9,12	16,16	7,7	11,11	12,12

Table 10. STR cell line identification of the ABC-1-LT cell line. STR analysis of the ABC1-LT cell line using the online DSMZ database. The evaluation value (EV) was calculated as in Table 10. The table shows cell lines identified with an EV > 0.7 relative to the ABC1-LT cell line. Numbers in red indicates STR lengths that diverge from the ABC-1-LT cell line.

			STR locus								
			AM	**D5S818**	**D13S317**	**D7S820**	**D16S539**	**vWA**	**TH01**	**TPOX**	**CSF1PO**
Evaluation Value	**Cell line No.**	Query: **ABC-1-LT**	*X,X*	*11,13*	*8,11*	*8,10*	*13,13*	*16,22,23*	*6,1*	*11,11*	*8,10*
0.92(34/37)	CRL-2781	p53R [JHU-56]	X,X	11,13	8,11	8,10	12,13	16,22	6,10	11,11	8,10
0.84(32/38)	CRL-2577	RKO	X,X	11,13	8,11	8,10	12,13	15,16,17	6,10	11,11	8,10
0.76(28/37)	CRL-2579	RKO-AS45-1	X,X	11,13	8,11	8,10	12.1,13	16,24	6,10	10,11	8,11

Thus, for the ABC-l-LT cells all the best matching cell lines from the STR identification were related to RKO cells (**Table 10**). Interestingly RKO cells have a shorter doubling time than ABC-1 cells (21 versus 72 hours, respectively [80] and in addition RKO cells are known to be insensitive to growth inhibition by G007-LK treatment. Given the facts above together with the unsuccessful attempts to reproduce the generation of ABC-1-LT cells from a new batch of ABC-1 cells we conclude that the ABC-1-LT cell line that originally was thought to be derived due to adaptive responses of the ABC-1 cell line to long term DMSO treatment rather is a contamination of RKO cell present in the old batch of ABC-1 cells. Both ABC-1 and RKO cells have been cultivated at the same time previously in the Krauss lab and a contamination of the old ABC-1 cells with small amounts of RKO cells is possible. During long time cultivation of a ABC-1 cell line contaminated with small amounts of RKO cells the RKO cells would eventually outgrow the ABC-1 cells and become the predominant cell type in the culture. Such a scenario would also explain the ABC-1-LT cells change in morphology and resistance to growth inhibition to G007-LK treatment. Based on the conclusion above the original aim of this Thesis to use the isogenic ABC-1 and ABC-1-LT cell pair to investigate the molecular mechanisms underlying sensitivity to growth inhibition to G007-LK treatment was abandoned.

4. 2

Part II: Analysis of WNT/β-catenin independent cellular consequences of tankyrase inhibition in the RKO cell line that is insensitive to growth inhibition by G007-LK treatment.

The main rationale for using tankyrase inhibitors as anticancer agents is inhibition of WNT/β-catenin signaling thus leading to reduced growth rates of the cancer cells. However, tankyrases are multifunctional proteins with important roles in many cellular processes (see Introduction) and for safe development of tankyrase inhibitors as therapeutic agents it is important that all potential effects that tankyrase inhibition can cause on the targeted cells are characterized. In the second part of this Thesis we wanted to analyze effects of tankyrase inhibition by using the colorectal cancer cell line RKO as a model system. Proliferation of RKO cells is independent of WNT/β-catenin signaling and treatment of RKO cells with the G007-LK tankyrase inhibitor does not influence on their growth rates [29, 81]. Consequently RKO cells present an attractive model system for investigating WNT/β-catenin independent functions of tankyrase inhibition.

4.2.1 Analysis of gene expression changes in G007-LK treated RKO cells by RNA sequencing

In another project in the Krauss lab, RNA sequencing on RKO cells treated for 24 hours with either DMSO or 1 μM G007-LK had already been performed. The results from the RNA sequencing were used to generate a heatmap that shows the differentially expressed genes that was most significant changed upon G007-LK treatment (**Figure 11)**. Interestingly, gene ontology (GO) term enrichment analysis revealed that five of the genes (*MSMO1*, *CYP51A1*, *DHCR7*, *INSIG1*, *HMGCS1*) that were most significantly changed upon G007-LK treatment were associated with the GO term "cholesterol biosynthetic process". In addition the *STARD4* gene was associated with GO terms related to cholesterol transport and storage ("cholesterol import", "cholesterol transport involved in cholesterol storage", "intracellular cholesterol transport"). The transcription of the genes involved in cholesterol biosynthesis

(*CYP51A1*, *MSMO*, *INSIG1*, *HMGCS1* and *DHCR7*) was all up regulated in the G007-LK treated cells, thus indicating that inhibition of tankyrase activity in RKO cells resulted in increased cholesterol synthesis.

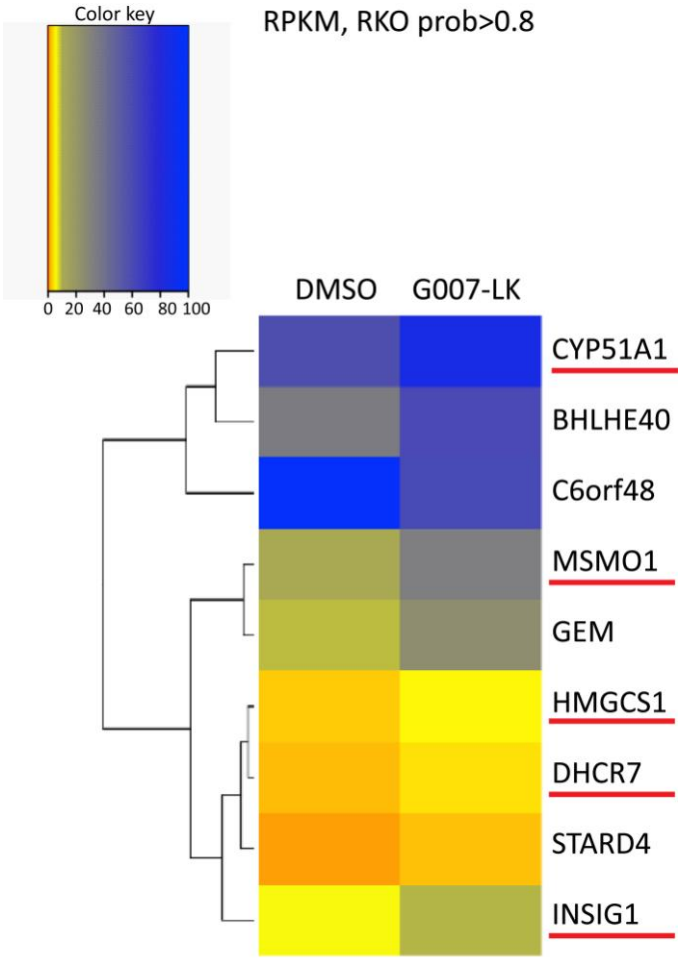

Figure 11. **Heatmap of protein coding genes displaying significant changed expression upon G007-LK treatment of RKO cells.**

The heatmap shows protein coding genes that were significant changed in RKO cells upon treatment with 1 μM G007-LK for 24 hours (versus the DMSO treatment control). Differentially expressed genes were detected with the NOIseq method and shown are genes with a probability>0.8 [67]. Red color indicates low expression and blue color indicate high expression as indicated in the color key. Underlined are genes identified by GO term enrichment analysis to be associated with the GO term "cholesterol biosynthetic process" identified by DAVID [82] using the Biological Process annotation (GOTERM_BP_DIRECT).

4.2.2 Analysis of mRNA expression levels of genes identified by RNA sequencing to be differentially expressed in RKO cells in response to G007-LK treatment.

To verify the results from the RNA sequencing data, identifying genes differentially expressed upon 24 hours G007-LK treatment, quantitative real time PCR (qRT-PCR) analysis of mRNA levels was performed on four of selected genes (*MSMO1*, *DHCR7*, *INSIG1*and *CYP51A1*). All of the genes selected for qRT-PCR analysis are involved in the cholesterol biosynthesis, and three (*CYP51A1*, *MSMO* and *DHCR7*) of the genes encode proteins that are directly involved in the final steps of the synthesis (**Figure 12A**). As seen in **Figure 12B**, all the transcription levels of all of the selected genes was significantly increased in response to G007-LK treatment ranging from 2.34 fold increase of *CYP51A1* to 3.56 fold increase of *MSMO1* mRNA levels. The results correspondent well with the RNA sequencing data thus verifying the influence of G007-LK treatment on transcription of genes involved in the cholesterol synthesis pathway.

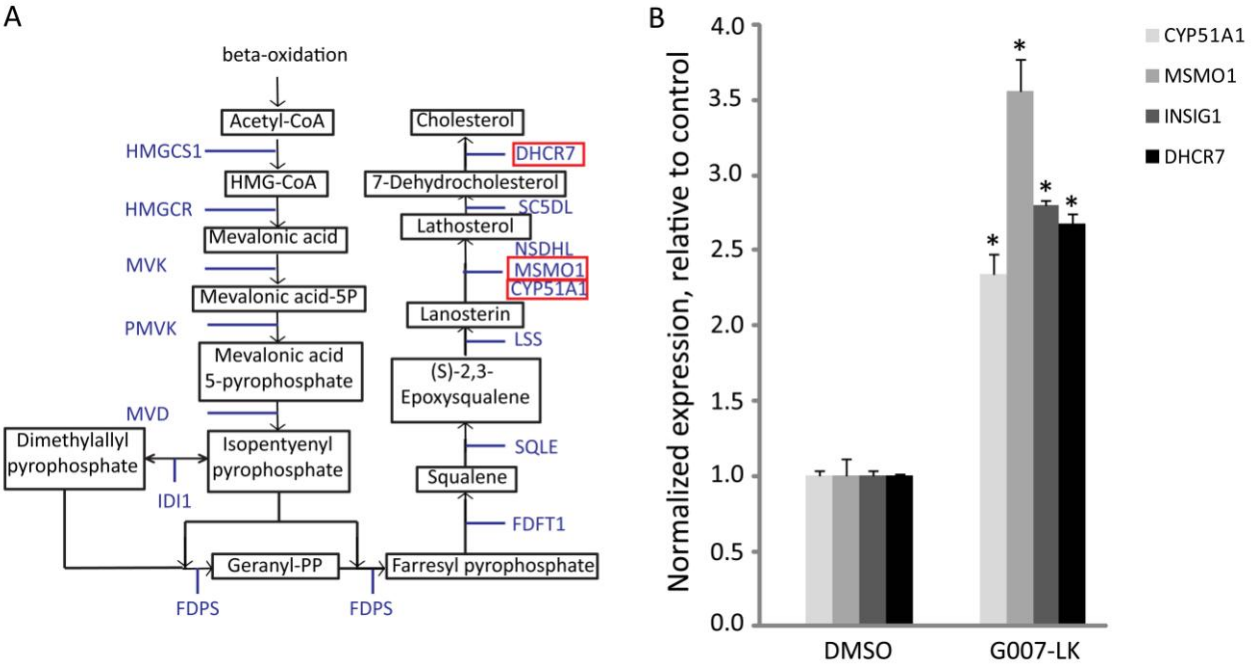

Figure 12. qRT-PCR analysis of mRNA levels of selected genes involved in cholesterol biosynthesis in DMSO and G007-LK treated RKO cells.

A) Schematic illustration of the cholesterol biosynthesis pathway. Three of the genes selected for qRT-PCR analysis (*CYP51A1*, *MSMO* and *DHCR7*) are involved in the final step of the pathway as indicated. Enzymes

required for each specific step in the pathway are written in blue. The figure is adapted from Robertson *et al.* [83]

B) qRT-PCR analysis of *MSMO1*, *DHCR7*, *INSIG1*and *CYP51A1* mRNA levels in DMSO and G007-LK treated RKO cells. Asterix indicates p value < 0.0001 (unpaired t test).

4.2.3 Measurement of cellular cholesterol levels in DMSO and G007-LK treated RKO cells

Given that several genes involved in the cholesterol biosynthesis pathway displayed increased expression upon G007-LK treatment we next analyzed if the levels of cellular cholesterol was changed upon G007-LK treatment of RKO cells. Labeling of cellular cholesterol was performed by Filipin staining and as seen in **Figure 13A** compared to the DMSO control, G007-LK treatment led to increased levels of cholesterol in RKO cells. As a control for the Filipin staining cells grown in lipid-depleted (LD) medium containing an inhibitor of cholesterol synthesis was included. The observed decreased staining intensity of cells grown in LD medium (versus DMSO treated cells) verified the applicability of Filipin staining to detect changes in cellular cholesterol levels. With all treatments the localization of cholesterol was mainly at cell membrane. However, some cholesterol was also observed in cytoplasmic areas and in the G007-LK treated cells there was an increased accumulation of cholesterol in these cytoplasmic areas (**Figure 13A**).

To quantify changes in cellular cholesterol levels flow cytometric analysis of Filipin stained cells was carried out. As seen in the histograms in **Figure 13B** the flow cytometric analysis could detect changes in the mean fluorescence intensity of Filipin stained G007-LK, DMSO and LD medium treated cells. Compared to DMSO treatment, G007-LK lead to a significant 1.5 fold increase while cells grown in LD medium displayed significant 2.1 fold decrease in mean fluorescence intensity (**Figure 13C**).

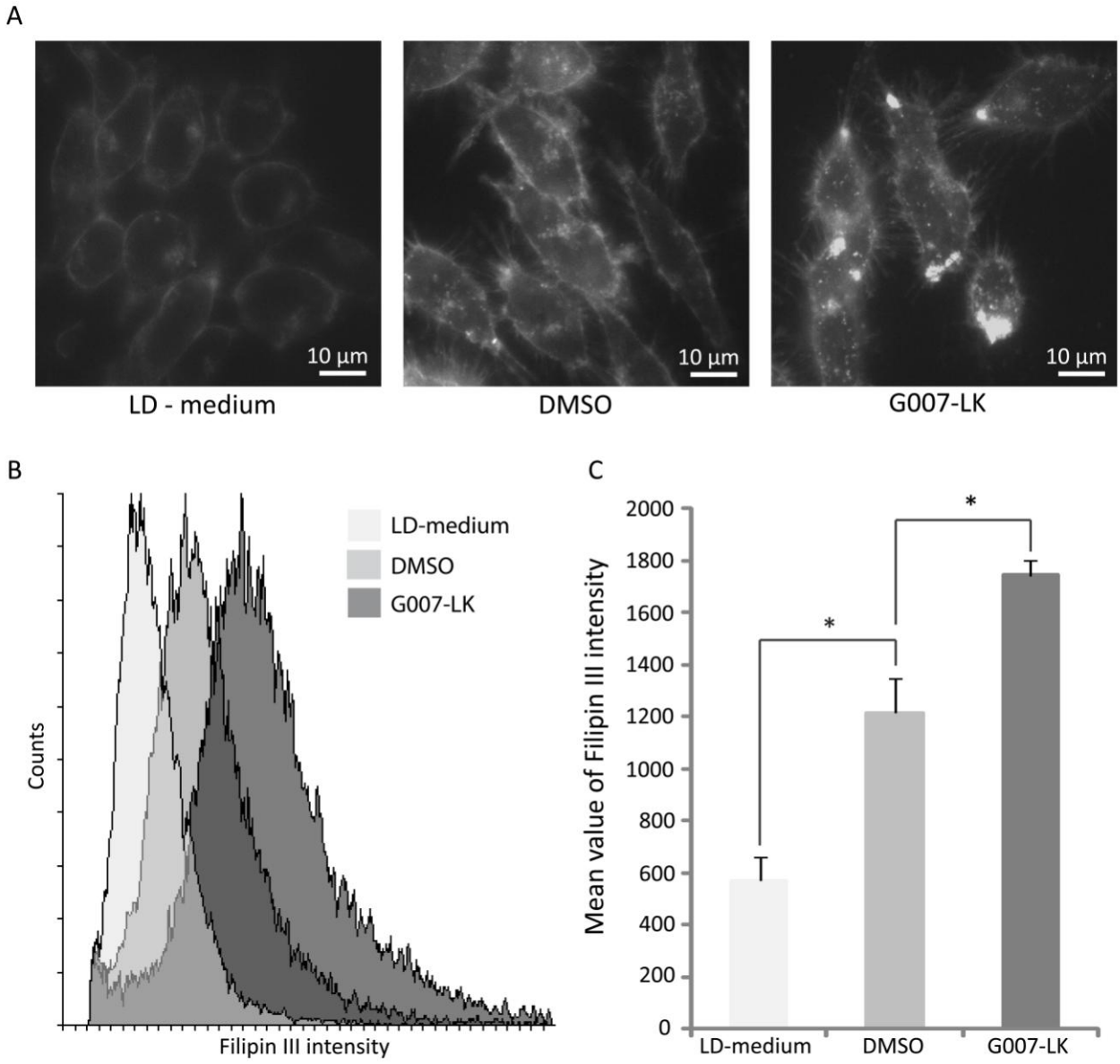

Figure 13. Analysis of cholesterol levels in DMSO, G007-LK and LD medium treated RKO cells by fluorescence microscopy and flow cytometry.

A) Representative images of Filipin fluorescence staining of free cholesterol in RKO cells treated with 1 µM G007-LK , 0.01 % DMSO or incubated with LD-medium for 24 hours as indicated.

B) Flow cytometric histogram showing the mean fluorescence intensity of Filipin fluorescence staining of free cholesterol in RKO cells treated as in A.

C) Bar graph representation of the flow cytometric analysis in B. Shown is mean values from three parallels with error bars representing standard deviation. Asterix indicates p value < 0.008 (unpaired t test).

4.2.4 Investigation of mechanisms underlying increased cellular cholesterol in RKO cells

4.2.4.1 Identification of common upstream regulators by Ingenuity pathway analysis (IPA) of the RNA sequencing results from DMSO and G007-LK treated RKO cells

To investigate mechanisms causing the increased levels of cellular cholesterol in RKO cells ingenuity pathway analysis (IPA) was done. IPA is a software application that can be used to find the main biological processes associated with the gene expression changes identified from for example a RNA sequencing analysis.

IPA pathway analysis revealed that the four most probable signaling networks underlying the gene expression changes observed in RKO cells upon G007-LK treatment was related to cholesterol biosynthesis (**Figure 14**). Furthermore in the list of predicted upstream regulators responsible for the observed gene expression changes identified SREBF-2 and SREBF-1 as top candidates (**Table 11**).

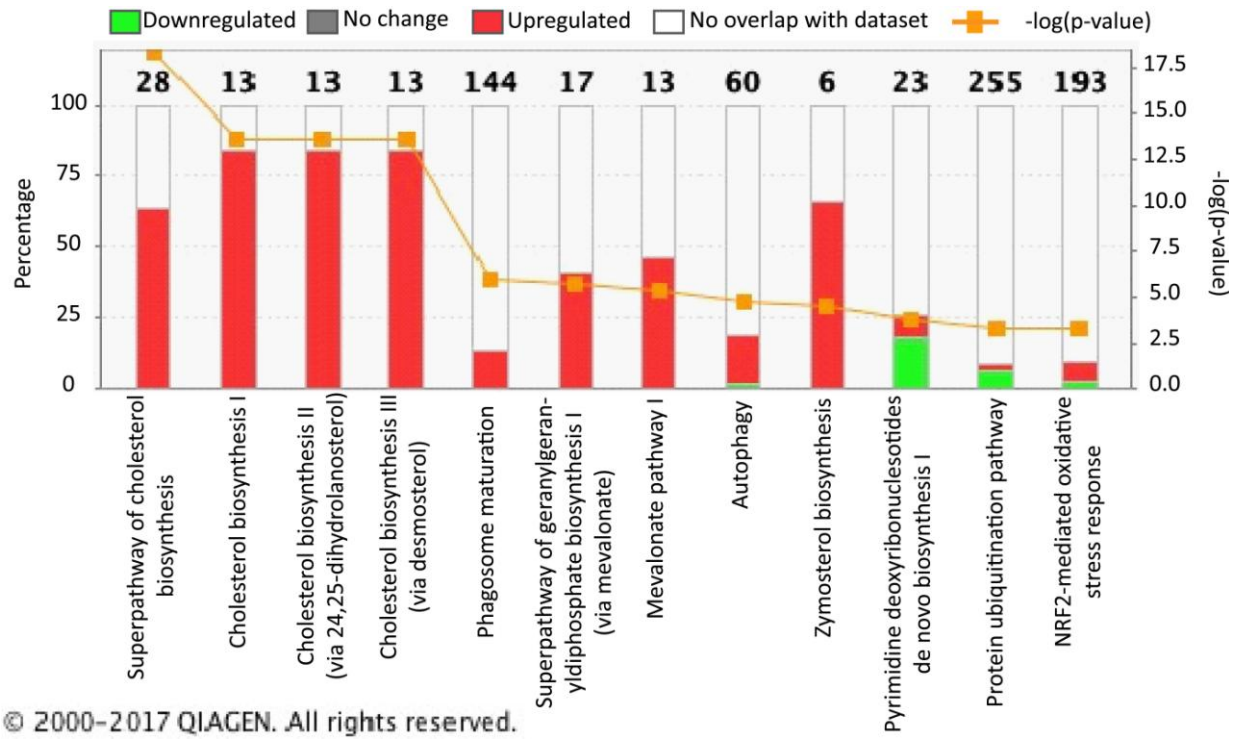

Figure 14. IPA pathway analysis identifying cholesterol biosynthesis pathways as most significantly associated with the gene expression changes observed in G007-LK treated RKO cells. The IPA was based on the top1000 most significantly regulated genes in G007-LK treated RKO cells as determined by the NOIseq method. The numbers above each bar represent number of genes identified in the data set to be associated with the particular pathway.

Table 11. Ingenuity Pathway Analysis (IPA) of the 1000 most differentially regulated genes from the RNA sequencing dataset. The table shows genes identified as possible upstream regulators, that were regulated in the dataset, ranked by "p-value of overlap". The "p-value overlap" is calculated using Fisher's Exact Test and measures whether there is a statistically significant overlap between the dataset genes and the genes that are regulated by a tanscritional regulator. The calculated z-score reflects the overall predicted activation state of the regulator where z-scores greater than 2 (activation) or smaller than-2 (inhibition) can be considered significant.

Upstream Regulator	Protein Name	Expr Log Ratio	Molecule Type	Predicted Activation State	Activation z-score	p-value of overlap
SREBF2	Sterol regulatory element-binding protein 2	0.365	transcription regulator	Activated	5.065	5.45E-28
SREBF1	Sterol regulatory element-binding protein 1	0.171	transcription regulator	Activated	5.325	4.29E-16
NFKBIA	NF-kappa-B inhibitor alpha	0.203	transcription regulator	Activated	2.358	9.34E-07
EGR1	Early growth response protein 1	0.105	transcription regulator	Activated	2.068	8.51E-06
MLX	Max-like protein X	0.109	transcription regulator	Activated	2.391	9.08E-06
LPIN1	Phosphatidate phosphatase LPIN1	0.266	phosphatase	Activated	2.190	1.47E-04
IRF7	Interferon regulatory factor 7	0.384	transcription regulator	Activated	2.226	6.68E-02

4.2.4.2 Analysis of localization of TNKS at Golgi apparatus upon G007-LK treatment in RKO cells

To determine the cellular localization of tankyrase IF was performed in DMSO and G007-LK treated RKO cells. As seen in **Figure 15** low levels of tankyrase could be observed scattered in the cytoplasm of DMSO treated cells. However upon G007-LK treatment the localization of tankyrase was changed to accumulation in defined areas in the cytoplasm near the nucleus. The levels of tankyrase were also increased in the G007-LK treated cells. Given that SREBPs was identified by the IPA as potential upstream regulators (**Table 11**) and that the Golgi apparatus is the site of SREBP activation, it was next investigated if the localization of tankyrase in G007-LK treated cells co-localized with the Golgi apparatus. Staining of cells using two independent markers (anti-GM130 and HPA) for the Golgi apparatus showed that the localization of tankyrase in G007-LK treated cells overlapped with the Golgi apparatus.

The accumulation of tankyrase in cluster at the Golgi apparatus upon G007-LK treatment of RKO cells would be compatible with an interaction of tankyrase with the SREBP activation step at the Golgi apparatus.

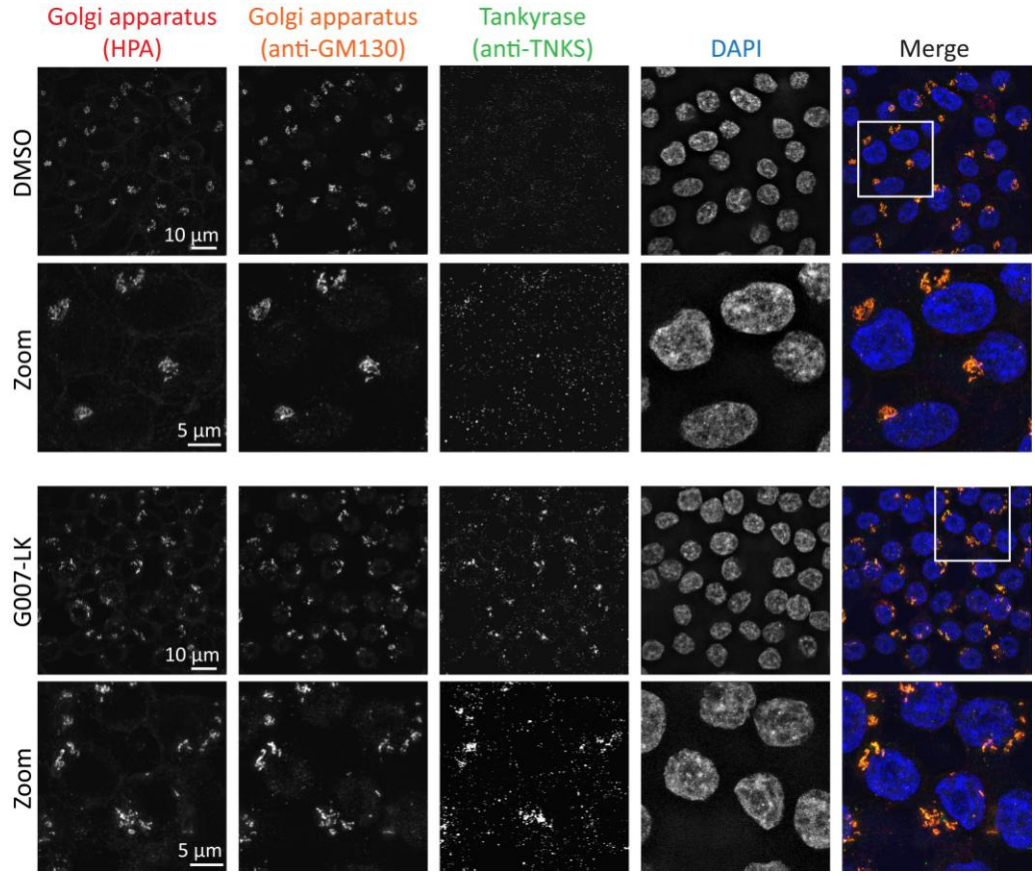

Figure 15. The localization of Tankyrase with G007-LK treatment.

Representative SIM images of RKO cells treated with 1 µM G007-LK or 0.01 % DMSO, as a control, for 24 hours. The cells were stained with two independent markers for the Golgi apparatus (HPA and GM130) and tankyrase as indicated. Nuclear counterstaining was performed with DAPI. The rectangle in the merged image indicates the area that is shown enlarged in the lower row of each treatment (Zoom).

4.2.4.3 Analysis of SREBP1/2 activation with G007-LK treatment in RKO cells.

Expression of cholesterol synthesis genes are regulated by the SREBP-1/2 transcription factors in a process where SREBP-1/2 are activated at the Golgi, translocate to the nucleus and induce expression of SRE regulated genes. With the aim of analyzing if tankyrase inhibition influenced on SREBP activation WB analysis of SREBP protein levels in DMSO and G007-LK treated cells was performed. To control for antibody specificity total cell lysates from RKO cells that had been transfected with expression constructs for the activated N-terminal parts of SREBP-1a, 1c and SREBP-2 was included. As seen in **Figure 16A**, SREBP-1 could not be detected in DMSO or G007-LK treated cells. However, SREBP-1 could neither be detected in control cells that that had been transfected with the SREBP-1a and -1c overexpression construct thus indicating that the SREBP-1 antibody used was unable to detect SREBP in our experimental set up. In WB using the SREBP-2 antibody, two bands were detected in all samples analyzed (**Figure 16B**) however neither of the bands did correspond with the given molecule weight of the precursor SREBP-2 (125kDa) or mature SREBP-2 (68 kDa). The smallest of the bands detected by the SREBP-2 antibody displayed a molecular weight between 65 kDa and 50 kDa which is close to the size of the mature SREBP-2 (68 kDa), however the intensity of the band was not increased in the cells that had been transfected with the SREBP-2 over expression construct thus indicating that the SREBP-2 did not work in our experiments. To verify the functionality of the expression constructs and transfection conditions WB using antibodies towards the FLAG tag included in the overexpressed SREBP proteins was done. As seen in **Figure 16C** WB using the anti-FLAG antibody could detected bands with the predicted molecular weight only in cells that had been transfected with the expression constructs for activated SREBP-1a, SREBP-1c and SREBP-2.

In conclusion we could not determine if G007-LK treatment of RKO cells influenced on SREBP protein levels this due inability of the SREBP antibodies tested to detect SREBP proteins. One additional SREBP-1 and two additional SREBP-2 antibodies were also tested in WB analysis, however as shown in **Supplementary Figure S1**, none of the antibodies tested could detect SREBP-1 or SREBP-2 proteins.

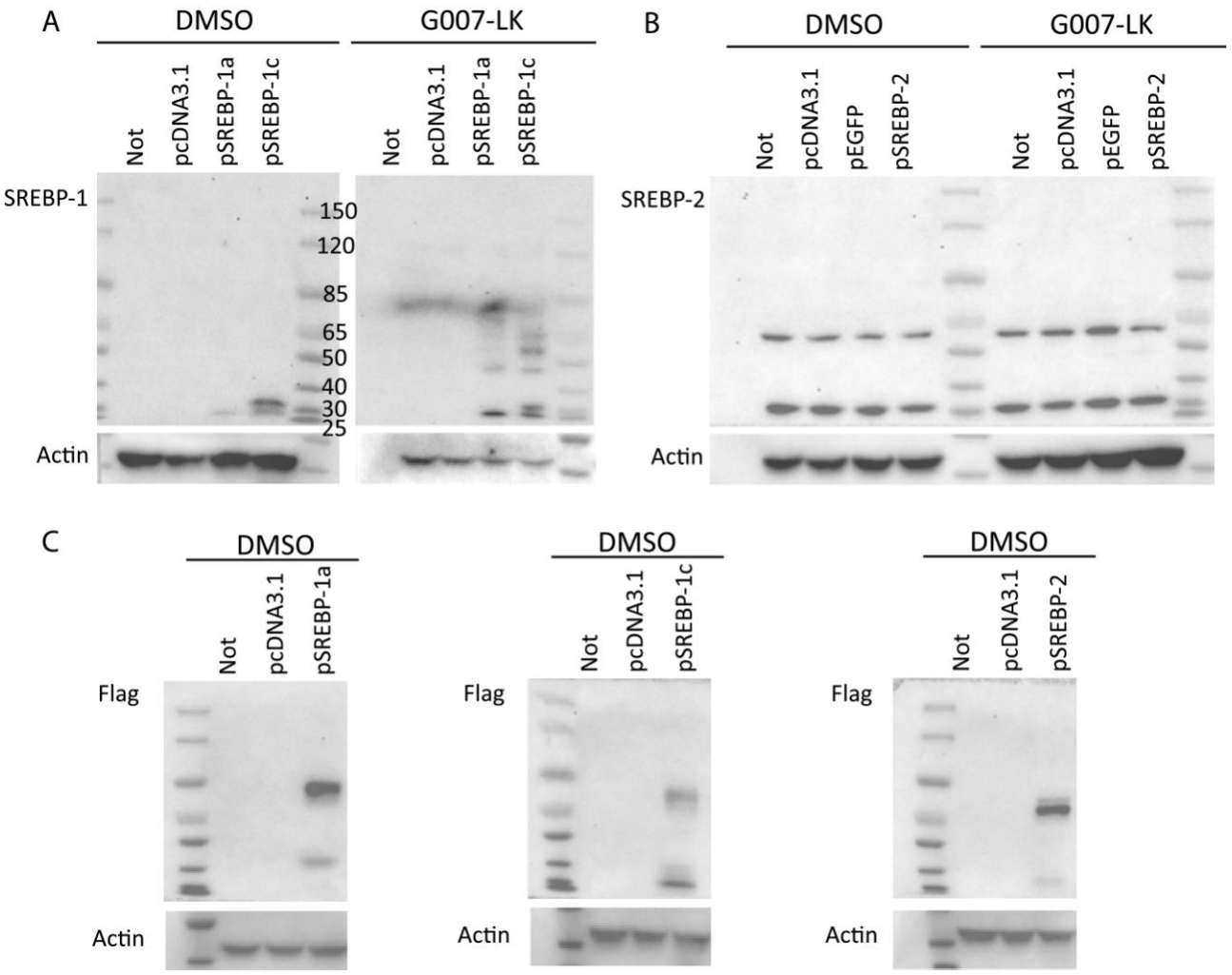

Figure 16. Western blot analysis of α-SREBP-1, α-SREBP-2 and transfected cells with α-Flag.

A) WB analysis of SREBP-1 (using the Sc-17755 ab) on total cell lysates from DMSO and G007-LK treated cells that that were untransfected (not) or transfected with pcDNA3.1 (control) or with the expression constructs pSREBP-1a and pSREBP-1c as indicated. Detection of β-actin was used to control for loading and protein transfer. The molecular weight of the bands in the protein size marker is indicated. The same protein size marker was included in all blots.

B) WB analysis of SREBP-2 (using the ab-30682 ab) on total lysate from RKO cells treated as in A with the exception that the cells had been transfected with the expression construct pSREBP-2 as indicated.

C) WB analysis using the anti-FLAG antibody on total lysate DMSO treated cells transfected with the pcDNA3.1 (control)

As an alternative strategy to measure if SREBP activity was influenced by G007-LK treatment, reporter gene assays using constructs containing SRE controlled luciferase expression was done. The first reporter construct tested was the pSynSRE-T-Luc that consists of a hamster HMG-CoA synthase promoter sequence containing 2xSRE elements and a minimal HMG-CoA synthase TATA box. RKO cells were transfected with the reporter construct, pRenilla and pEGFP, and treated with G007-LK, DMSO as a control or kept untreated (not). To monitor which of the SREBPs isoforms that activate the reporter construct, the cells was also co transfected with the pSREBP-1a, pSREBP-1c or SREBP-2 overexpression constructs in addition to the reporter construct and pRenilla internal control construct. As seen in **Figure 17A** the luciferase expression from the pSynSRE-T-Luc construct was significantly increased upon G007-LK treatment compared to both the untreated and the DMSO treated cells. The pSynSRE-T-Luc construct was activated upon co transfection with the pSREBP-1a and pSREBP-1c expression constructs however the SREBP-2 construct did not influence on the pSynSRE-T-Luc activity. Given that SREBP-2 is the isoform that have the most to do with the cholesterol synthesis[84] a second SRE-luc reporter construct was also analyzed for potential activation by G007-LK treatment. The second reporter construct, pSRE-Luc, consist of 3 tandem copies of repeats 2 and 3 of the human LDL receptor promoter, and incorporates three SRE elements. As seen in **Figure 17B**, G007-LK treatment of pSRE-Luc transfected cells did not result in a significant activation of luciferase expression compared to untreated or DMSO treated cells. The pSRE-Luc construct was strongly activated upon co transfection with pSREBP-1a, no activation was observed upon co transfection with pSREBP-1c and pSREPB-2 expression constructs.

In summary G007-LK treatment did activate SRE driven transcription in one of the two SRE reporter gene constructs tested. However, although statistically significant the G007-LK mediated activation of the pSynSRE-T-Luc construct was moderate compared to the activation level observed with pSREPB-1a over expression. The observation that neither of the SRE reporters tested was activated upon co transfection with the pSREBP-2 overexpression constructs indicate that neither of the SRE reporters was optimal for analyzing SREBP-2 mediated activation of cholesterol synthesis.

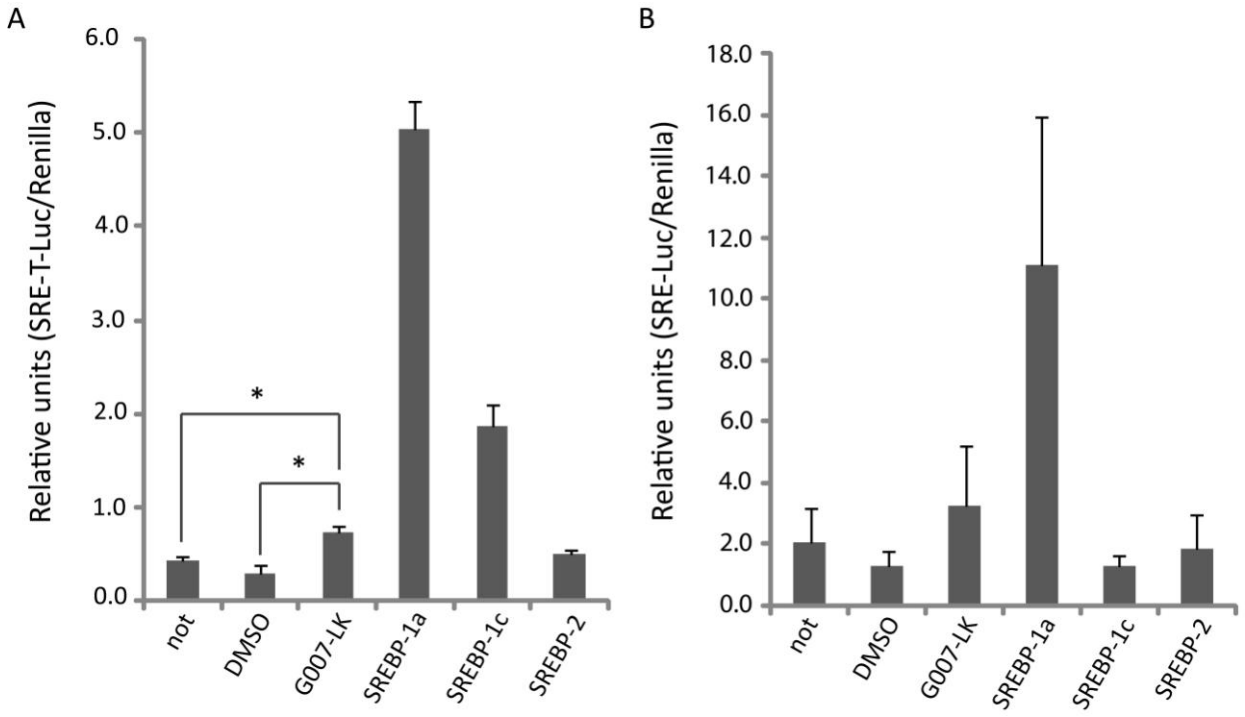

Figure 17. Analysis of the SRE-promoter activity upon G007-LK treatment.

A) Promoter construct one: untreated cells, cells treated with 1 μM G007-LK and cells grown in 0.01 % DMSO (control) was transfected with pSynSRE-T- Luc, pRenilla and pEGFP. To investigate the respond of the promoter to the different isomforms, untreated cells was transfected with the pSynSRE-T-Luc, pRenilla and each of the isoforms (pSREBP-1a, pSREBP-1c and pSREBP-2). Show are mean values from three parallels with error bars representing standard deviation. Asterix indicates p value < 0.02 (unpaired t test)

B) Promoter construct two: untreated cells, cells treated with 1 μM G007-LK and cells grown in 0.01 % DMSO (control) was transfected with pSRE- Luc, pRenilla and pEGFP. To investigate the respond of the promoter to the different isomforms, untreated cells was transfected with the pSynSRE-T-Luc, pRenilla and each of the isoforms (pSREBP-1a, pSREBP-1c and pSREBP-2). Mean values from three parallels with error bars representing standard deviation are show also here.

4.2.5 Analysis of functional consequences of increased cellular cholesterol levels in RKO cells

4.2.5.1 Fluorescent microscopy analysis of golgi, mitochondria morphology together with lipid rafts in DMSO and G007-LK treated RKO cells.

It has been reported that increased levels of cellular cholesterol can induce increased vesiculation and dispersal of the Golgi apparatus vesicles [85]. Cholesterol has been reported to accumulate in the mitochondria and such accumulation has been associated with higher cell proliferation and tumor growth. Furthermore, the metabolic conditions inside the mitochondria are reported to be reflected by the structure of the mitochondria [86, 87]. Lipid rafts are microdomains of the plasma membrane that are enriched in cholesterol and sphingolipids, where cholesterol is the dynamic glue that holds the rafts together [54]. Lipid rafts are known to be involved in trafficking of intracellular signaling molecules and regulation of receptor trafficking.

The morphology of the Golgi apparatus and mitochondria together with changes in amounts of lipid rafts was investigated by fluorescent markers for each of the organelles upon G007-LK treatment and DMSO treated RKO cells. As seen in **Figure 18** while the morphology of the mitochondria was unchanged upon G007-LK treatment, the Golgi apparatus was more fragmented upon G007-LK treatment, compared to the DMSO control where the Golgi apparatus displayed a more tightly packed morphology. The fluorescent labeling of lipid rafts to cells treated with G007-LK, compared to the DMSO control displayed increased amounts of lipid rafts at the plasma membrane.

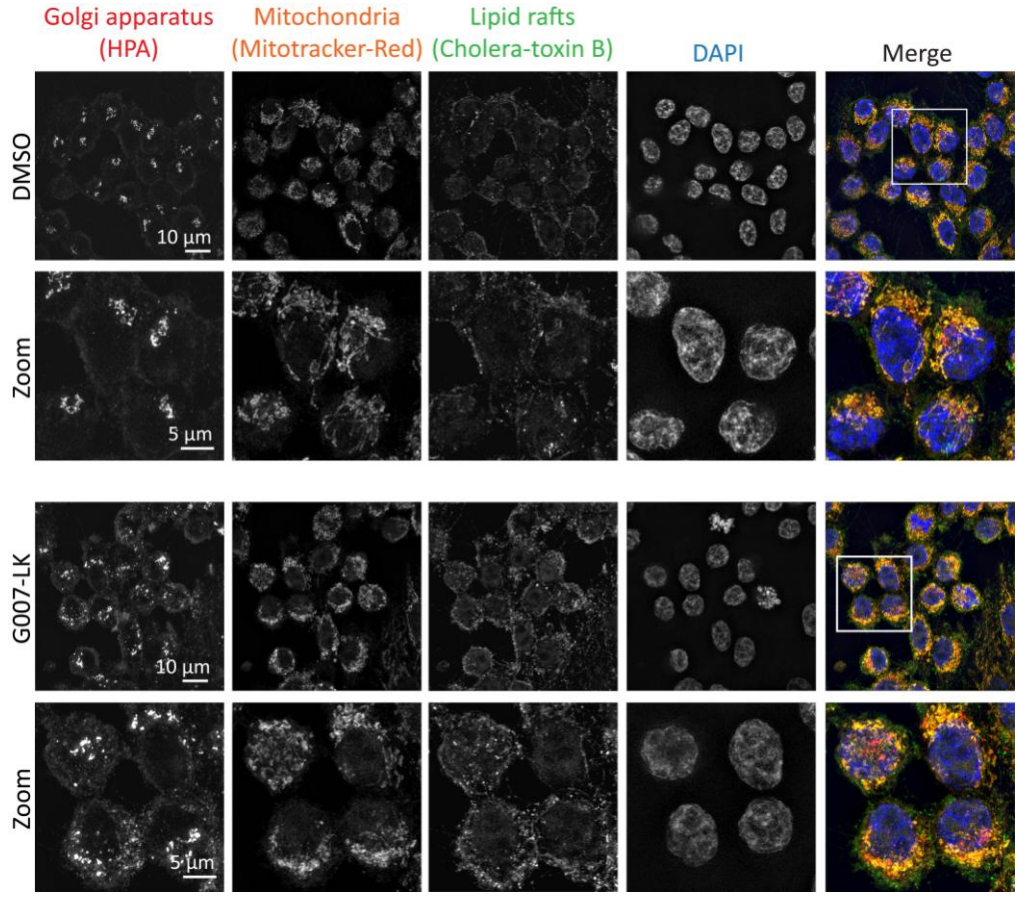

Figure 18. Analysis of Golgi apparatus, mitochondria and lipid rafts in G007-LK treated cells. Representative SIM images of RKO cells treated with DMSO and G007-LK. The cells were stained for fluorescent markers for the Golgi apparatus, mitochondria and lipid rafts as indicated. DAPI was used for nuclear staining. The rectangle in the merged image indicates the area that is shown enlarged in the lower row

4.2.5.2 Quantification of oxysterol levels in DMSO and G007-LK treated RKO cells.

Oxysterols are oxygenated derivates of cholesterol and when cholesterol levels are high increased levels of oxysterols can be generated [88]. To investigate if the G007-LK mediated cholesterol increase influenced on oxysterol levels, mass spectrometry (MS) quantification of 24(S)-hydroxycholesterol (24S-OHC), 25-hydroxycholesterol (25-OHC) and 27-hydroxycholesterol (27-OHC) was performed on untreated, DMSO and G007-LK treated RKO cells. As seen in **Figure 19** the levels of 27-OHC was not significant changed upon G007-LK treatment. On the contrary the levels of 24S-OHC and 25-OHC were significant increased upon G007-LK treatment, compared to both the untreated and the DMSO treated RKO cells.

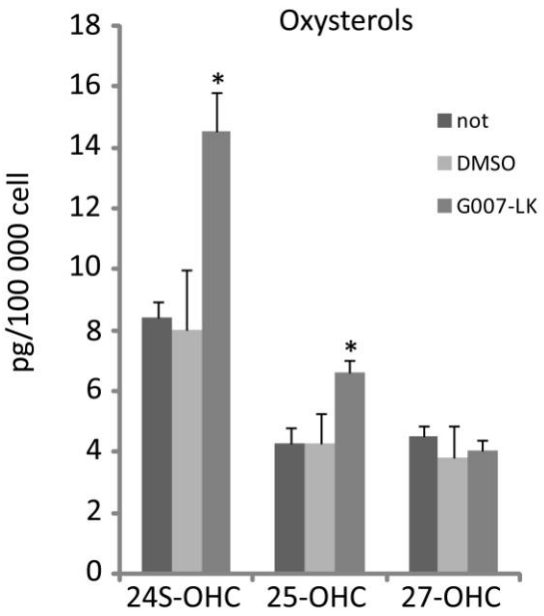

Figure 19. MS quantification of oxysterols in untreated, DMSO and G007-LK treated RKO cells.

MS quantification of the oxysterols 24(S)-hydroxycholesterol (24S-OHC), 25-hydroxycholesterol (25-OHC) and 27-hydroxycholesterol (27-OHC) in untreated, DMSO and G007-LK treated RKO cells as indicated. Shown are mean value from three parallels with error bars representing standard deviation. Asterix indicates p value < 0.02 (unpaired t test).

5 Discussion

5.1

Part I: Identifying a RKO cell line contamination in G007-LK resistant long term DMSO treated ABC-1 cells.

In the first part of this work the initial goal was to use the ABC-1 WT and ABC-1-LT cell lines as tools for investigating mechanisms that define sensitivity to growth inhibition in response to treatment with the G007-LK tankyrase inhibitor. It had been previously been established that the lung cancer ABC-1 WT cell line was sensitive to growth inhibition by G007-LK treatment [77]. The ABC-1-LT cell line had been established by long term treatment of ABC-1 WT cells with 0.001 % DMSO. Given that the ABC-1 and ABC-1-LT cells were considered to be isogenic cell lines with opposite sensitivity to G007-LK treatment they presented an attractive model system for investigating mechanisms regulating sensitivity to G007-LK treatment. Although the generation ABC-1-LT cells had been derived repeatedly from ABC-1 WT cells by long term DMSO treatment, in my hands the generation of ABC-1-LT cells could not be reproduced under similar conditions. Thus, after 30 passages of ABC-1 WT cells in the presence of 0.001 % DMSO the characteristic morphological changes described in ABC-1-LT cells could not be observed (**Figure 10**). In a search for possible differences between the used materials and methods, it was observed that different batches of ABC-1 cells were used in the previous work and in my work. In particular, for the here reported work a new batch of ABC-1 WT cells newly arrived from the supplier was used.

When STR analysis was performed on the cells used in the previous work, and the new batch of ABC-1 WT cells used in the current work, both cell lines displayed identical STR profiles (**Table 8**) and were identified to be ABC-1 cells (**Table 9**). In contrast, the ABC-1-LT cell line that was derived after long term treatment in DMSO displayed a STR profile that deviated from the ABC-1 WT cells at 20 of the STR loci with only the AM sex determination marker being identical (**Table 8**). This demonstrated that the ABC-1 and ABC-1-LT cell lines were completely unrelated. The STR profile showed that the ABC-1-LT cell line was most related to the colon carcinoma RKO cell line (**Table 9**). From these date it was concluded that a the old batch of ABC-1 WT cells probably had been contaminated with a

small amount of RKO cells that during the long time cultivation in 0.001 % DMSO outgrow the ABC-1 cells and become the predominant cell type in the culture. Given that RKO displays higher proliferation rates, have a more fibroblastic morphology than ABC-1 cells and are insensitive to G007-LK treatment this would explain the observed features (Figure 9) of the proposed ABC-1-LT cell line.

Cell line misidentification and cross contamination with other cell lines is a problem in scientific research laboratories word wide. In fact, it has been estimated that more that 15 % of human cell lines do not correspond to the claimed source [78]. Indeed, a single cell introduced from elsewhere may have the potential to outgrow the original culture within five passages [89]. Cross contamination can occur when several cell types are handled in incubators and tissue culture hoods. To avoid cell line cross contamination proper aseptic techniques and adequate separation of individual cell types during handling are important factors.

To deal with the wide spread problem of cell line misidentification and cross contamination the International Cell line Authentication Committee (ISLAC) was established in 2012 and in order to track all known cell cross contaminations they publish a Database of Cross Contaminated or Misidentified Cell Lines [90]. As highlighted in this work when a cell line is observed to change appearance and properties, STR profiling to verify the cell line identity is critical in order to avoid incorrect conclusions. The challenge with cell line misidentification and cross contamination has increasingly been acknowledged by the scientific community and an increasing number of scientific journals now require STR profiling of cell lines used upon acceptance of a manuscript.

5.2

Part II: Analysis of WNT/β-catenin independent cellular consequences of tankyrase inhibition in the RKO cell line that is insensitive to growth inhibition by G007-LK treatment.

Tankyrase inhibitors, like G007-LK, are explored as a therapeutic option for WNT/β-catenin driven cancer types [19, 91]. However, in addition to regulation of WNT/β-catenin signaling, tankyrases are also known to affect numerous additional cellular functions [18]. In the second part of this thesis, cellular consequences of tankyrase inhibition in the RKO cell line was analyzed. The proliferation of RKO cells is independent of WNT/β-catenin signaling and cell growth of RKO cells is unaffected by G007-LK treatment [29, 81] thus making this cell line an attractive model system for analysis of WNTβ-catenin independent consequences of tankyrase inhibition.

Increased cholesterol levels in RKO cells upon G007 treatment.

Analysis of global RNA sequencing of RKO cells with and without G007-LK treatment revealed that a significant number of the top scores of differentially regulated mRNAs were encoding proteins implied in cholesterol synthesis (Figure 11). Four of the genes shown in the RNA sequencing results to be up regulated by G007-LK treatment were chosen for confirmatory analysis by qRT-PCR. This analysis verified increased mRNA levels of CYP1A1, MSMO1, INSIG1 and DHCR7 upon G007-LK treatment. Filipin staining of free cholesterol was next performed to analyze whether an up regulation of cholesterol biosynthesis genes translated into increased levels of cellular cholesterol. As seen in **Figure 13,** RKO cells that had been incubated with G007-LK displayed a marked increase of cellular cholesterol levels compared to DMSO treatment. Cholesterol in the treatment group was seen at the cell membrane and in intracellular “aggregates”.

The cellular level of cholesterol levels can be regulated by several mechanisms including increased biosynthesis, increased uptake and decreased efflux [59]. In G007-LK treated RKO cells, the up-regulation of mRNAs related to cholesterol biosynthesis indicate

that the reason for the increased cholesterol levels was likely due to an increased cholesterol synthesis rather than increased uptake or decreased efflux.

Mechanisms underlying increased cholesterol levels upon G007-LK treatment of RKO cells

Ingenuity pathway analysis (IPA) of RNAomics data allows to predict common upstream regulators of significantly changed genes. In G007-LK treated RKO cells, SREBF-1 and SREBF-2 as top candidates for common up stream regulators (**Table 11**). SREBPs are transcription factors controlling the expression of numerous enzymes required for cholesterol, fatty acid and phospholipid synthesis [63]. IF analysis of the tankyrase along with a marker for the Golgi apparatus showed that upon G007-LK tankyrase accumulated in cluster that co-localized with the Golgi apparatus (**Figure 15**). The proteolytic cleavage of precursor SREPBs to activated SREBP occurs at the Golgi and the accumulation of tankyrase at this organelle in G007-LK treated cells might indicate that tankyrase might affect the activation step of the SREBP precursor.

Western blot analysis to detect changes in protein levels of activated SREBP upon G007-LK treatment could not detect endogenous full length or cleaved activated forms of SREBP (1a, 1c and 2) in RKO cells (**Figure 16**). Two different supposedly SREBP-1 recognizing antibodies and three SREBP-2 antibodies were tested, but none of the antibodies detected bands with the expected sizes of 68 kDa for mature SREBP and 125 kDa for precursor SREBP (**Figure 16**). The Western blot experiment was repeated several times with altered conditions (protein amounts and antibody incubation times), however, endogenous SREBP could not be detected. The reason why SREBP not could be detected could be related to antibody quality or due to low protein SREBP levels in RKO cells. Comparison of FLAG-tagged constructs with anti-FLAG and anti-SREBP gave bands at different size, which can indicate poor quality of the antibodies (**Figure 16**).

The reporter gene assays performed to investigate if G007-LK influenced SRE mediated transcriptional activation showed significant G007-LK mediated activation in one reporter construct while only a not significant tendency of G007-LK mediated activation using a second SRE reporter construct (**Figure 17**). Interestingly, control experiments based on a co-transfection of the SRE reporters with over-expression constructs for the activated

SREBP-1a, 1c and 2 isoforms showed that both the SRE reporter constructs were hardly activated by SREBP-2 co-tansfection. Given that the SREBP-2 isoform is reported to be relatively specific to regulating cholesterol synthesis [63] the lack of activation by SREPB-2 over-expression indicates that the two SRE reporter constructs were not optimal for analyzing the SREBP based activation of cholesterol synthesis genes. For further investigations, it would be necessary to identify – if present - a reporter construct that responds good to SREBP-2. Although we were unable to show convincing induction of SRE reporter constructs, a link between tankyrase and SRE activation has been reported by Chetterjee and colleagues in a publication where over-expression of a genome-wide cDNA library was performed to identify proteins that might affect the transcription of luciferase from the SREBP-specific SRE-promoter [92]. In the supporting information in Table S2 a complete list of validated repressors of the SREBP signaling pathway is included. Interestingly, tankyrase is listed as a repressor of the SREBP signaling pathway, this supports the scenario of increased cholesterol levels as a consequence of an inhibition of tankyrase by G007-LK. Our observation that inhibition of tankyrase activity leads to increased levels and the reported decrease of SRE activation in response to tankyrase over-expression indicates that tankyrases act as inhibitor of cholesterol synthesis.

Tankyrases are known to bind to proteins with the specific motif; RxxPDGxx [23]. Guettler and colleagues have described the structural basis and sequence rules for how tankyrases recognize their substrates. In the supplementary Table S4 all potentially proteins that can bind tankyrase is listed in a ranked list according to their tankyrase targeting score (TTS) in descending order. A search in this table of proteins involved in the SREBP signaling pathway, interestingly three motifs in SREBP-1 and one motif of SCAP matched for potentially binding sites to tankyrase. The TTS rank together with the protein and the binding motif is listed in **Table 12**. Interaction of tankyrase with SREBP-1 or SCAP could provide a link between G007-LK treatment and increased cellular cholesterol levels. However, preliminary results from analyzing a possible interaction between tankyrase and the predicted tankyrase binding peptides in SREBP-1 and SCAP have not been able to detect an interaction (Personal communication: Nai-Wen Chi, Department of Medicine, University of California San Diego).

Table 12. List of possible tankyrase interaction partners in the cholesterol biosynthesis pathway.

The table is adapted from supplementary table S4, Guettler *et al.*, 2011 [23].

TTS rank	Protein	Position	Peptide	TTS (p-value)
236	SCAP	820	RDSGVGSG	0.773 ($6.26e^{-02}$)
1519	SREBP1	446	RGSGSGGS	0.616 ($6.21e^{+00}$)
1809	SREBP1	1063	RRAGPGGK	0.610 ($7.30e^{+00}$)
6019	SREBP1	1064	RAGPGGKG	0.471 ($2.39e^{+02}$)

Cellular consequences of increased cholesterol levels

To investigate cellular consequences of increased cholesterol levels the morphology of Golgi, mitochondria and distribution of lipid rafts were analyzed (**Figure 17**). Compared to control cells the morphology of the Golgi apparatus in G007-LK treated cells displayed increased fragmentation. This is in agreement with Grimmer *et al.* who reported that the structure of the Golgi apparatus in HeLa cells were affected by increased levels of cholesterol by pronounced vesiculation and formation of smaller stacks [93]. Their results demonstrate that the vesiculation of the Golgi apparatus as a consequence of increased cholesterol is mediated by a cytosolic phospholipase A2 (PLA_2) and dynamin-dependent mechanism. It has been reported that increased cellular cholesterol can accumulate in the mitochondria [86], and that such an accumulation can lead to alteration of the mitochondrial architecture [94]. In G007-LK treated RKO cells the mitochondria did not display clear changes of morphology. For further investigations, it would be interesting to label both cholesterol and mitochondria to see if the cholesterol clumps from the Filipin staining are localized to the mitochondria. Analysis of the distribution of lipid rafts showed that the G007-LK treated RKO cells displayed increased levels of lipid rafts in the membrane. Cholesterol is known to be the main component in lipid rafts and it has been reported that increased levels of cholesterol can lead to increased amounts of lipid rafts and that such changes can influence cell signaling activities and membrane fluidity of the cells [54].

As a last consequence of increased cholesterol the oxysterol levels was analyzed, and RKO cells treated with G007-LK have an increased amount of two of the three oxysterols analyzed (**Figure 18**). Oxysterols are oxygenated derivates of cholesterol, which are intermediates in cholesterol excretion pathways [55]. The two oxysterols that showed increased amount was 25-hydroxycholesterol and 24S-hydroxycholesterol and these are

known to suppress cholesterol synthesis [95]. The major oxysterols in the circulation such as 24S-hydroxycholesterol changes their concentration in parallel with cholesterol [55]. The treatment of RKO cells with G007-LK leads to increased cholesterol levels, and since the concentration of oxysterols often changes in parallel with cholesterol concentration, the oxysterols can possible lead to down regulation of cholesterol levels in the cells. The results indicates that the oxysterols are increased, and for future work it would be interesting to see if the cholesterol levels are decreased again after 48, 72 or 96 hours. Also for further work it would be important to establish the generality of G007-LK mediated cholesterol increase, this by analyzing if G007-LK treatment influence on the cellular cholesterol levels in a panel of additional cell lines.

6 Conclusion

In conclusion our data showed that inhibition of tankyrase in the RKO cell line leads to accumulation of cellular cholesterol. The molecular target of tankyrase and the mechanism underlying increased cholesterol synthesis is not identified. As a consequence of G007-LK mediated increase in cholesterol levels RKO cells have more lipid rafts at the plasma membrane, displays fragmentation of the Golgi apparatus and contains increased amounts of 25-hydroxycholesterol and 24S-hydroxycholesterol.

The increased levels of cholesterol in response to tankyrase inhibition by G007-LK indicate that tankyrase may have a role in regulation of cellular cholesterol homeostasis that has not been described before. Characterization of all potential effects tankyrase inhibition might cause on targeted cells is important for the safe development of tankyrase inhibitors as therapeutic agents.

References

1. Hanahan, D. and R.A. Weinberg, *Hallmarks of cancer: the next generation.* cell, 2011. **144**(5): p. 646-674.
2. Cooper, G.M., *The Development and Causes of Cancer.* The Cell: A Molecular Approach. 2nd edition., 2000.
3. Hakim, D.N., et al., *Benign tumours of the bone: A review.* Journal of bone oncology, 2015. **4**(2): p. 37-41.
4. Komarova, N.L., A. Sengupta, and M.A. Nowak, *Mutation–selection networks of cancer initiation: tumor suppressor genes and chromosomal instability.* Journal of theoretical biology, 2003. **223**(4): p. 433-450.
5. Iurlaro, R., C.L. León-Annicchiarico, and C. Muñoz-Pinedo, *Regulation of cancer metabolism by oncogenes and tumor suppressors.* Methods Enzymol, 2014. **542**: p. 59-80.
6. Vogelstein, B. and K.W. Kinzler, *Cancer genes and the pathways they control.* Nature medicine, 2004. **10**(8): p. 789-799.
7. Vicente-Dueñas, C., et al., *Function of oncogenes in cancer development: a changing paradigm.* The EMBO journal, 2013. **32**(11): p. 1502-1513.
8. Sameer, A.S., *Colorectal cancer: molecular mutations and polymorphisms.* Frontiers in oncology, 2013. **3**.
9. Chung, D.C., *The genetic basis of colorectal cancer: insights into critical pathways of tumorigenesis.* Gastroenterology, 2000. **119**(3): p. 854-865.
10. Jasperson, K.W., et al., *Hereditary and familial colon cancer.* Gastroenterology, 2010. **138**(6): p. 2044-2058.
11. Kastrinos, F. and S. Syngal, *Inherited colorectal cancer syndromes.* Cancer journal (Sudbury, Mass.), 2011. **17**(6): p. 405.
12. Armelao, F. and G. de Pretis, *Familial colorectal cancer: a review.* World Journal of Gastroenterology: WJG, 2014. **20**(28): p. 9292.
13. Yamada, T. and M. Masuda, *The emergence of TNIK inhibitors in cancer therapeutics.* Cancer Science, 2017.
14. Anastas, J.N. and R.T. Moon, *WNT signalling pathways as therapeutic targets in cancer.* Nature Reviews Cancer, 2013. **13**(1): p. 11-26.
15. MacDonald, B.T., K. Tamai, and X. He, *Wnt/β-catenin signaling: components, mechanisms, and diseases.* Developmental cell, 2009. **17**(1): p. 9-26.
16. Clevers, H. and R. Nusse, *Wnt/β-catenin signaling and disease.* Cell, 2012. **149**(6): p. 1192-1205.
17. Huang, S.-M.A., et al., *Tankyrase inhibition stabilizes axin and antagonizes Wnt signalling.* Nature, 2009. **461**(7264): p. 614-620.
18. Haikarainen, T., S. Krauss, and L. Lehtio, *Tankyrases: structure, function and therapeutic implications in cancer.* Current pharmaceutical design, 2014. **20**(41): p. 6472-6488.
19. Riffell, J.L., C.J. Lord, and A. Ashworth, *Tankyrase-targeted therapeutics: expanding opportunities in the PARP family.* Nature reviews Drug discovery, 2012. **11**(12): p. 923-936.
20. Zhong, L., et al., *Nutritional energy stimulates NAD+ production to promote tankyrase-mediated PARsylation in insulinoma cells.* PloS one, 2015. **10**(4): p. e0122948.
21. Sbodio, J.I. and N.-W. Chi, *Identification of a Tankyrase-binding Motif Shared by IRAP, TAB182, and Human TRF1 but Not Mouse TRF1 NuMA CONTAINS THIS*

RXXPDG MOTIF AND IS A NOVEL TANKYRASE PARTNER. Journal of Biological Chemistry, 2002. **277**(35): p. 31887-31892.
22. Hsiao, S.J. and S. Smith, *Tankyrase function at telomeres, spindle poles, and beyond.* Biochimie, 2008. **90**(1): p. 83-92.
23. Guettler, S., et al., *Structural basis and sequence rules for substrate recognition by Tankyrase explain the basis for cherubism disease.* Cell, 2011. **147**(6): p. 1340-1354.
24. Yeh, T.-Y.J., et al., *Hypermetabolism, hyperphagia, and reduced adiposity in tankyrase-deficient mice.* Diabetes, 2009. **58**(11): p. 2476-2485.
25. Lupo, B. and L. Trusolino, *Inhibition of poly (ADP-ribosyl) ation in cancer: old and new paradigms revisited.* Biochimica et Biophysica Acta (BBA)-Reviews on Cancer, 2014. **1846**(1): p. 201-215.
26. Shammas, M.A., *Telomeres, lifestyle, cancer, and aging.* Current opinion in clinical nutrition and metabolic care, 2011. **14**(1): p. 28.
27. Ha, G., et al., *Tankyrase-1 function at telomeres and during mitosis is regulated by Polo-like kinase-1-mediated phosphorylation.* Cell Death & Differentiation, 2012. **19**(2): p. 321-332.
28. Zhang, H., et al., *Inhibition of tankyrase 1 in human gastric cancer cells enhances telomere shortening by telomerase inhibitors.* Oncology reports, 2010. **24**(4): p. 1059-1065.
29. Lau, T., et al., *A novel tankyrase small-molecule inhibitor suppresses APC mutation–driven colorectal tumor growth.* Cancer research, 2013.
30. Davis, A.J. and D.J. Chen, *DNA double strand break repair via non-homologous end-joining.* Translational cancer research, 2013. **2**(3): p. 130.
31. Dregalla, R.C., et al., *Regulatory roles of tankyrase 1 at telomeres and in DNA repair: suppression of T-SCE and stabilization of DNA-PKcs.* Aging (Albany NY), 2010. **2**(10): p. 691.
32. Curtin, N.J., *PARP inhibitors for cancer therapy.* Expert reviews in molecular medicine, 2005. **7**(4): p. 1-20.
33. Azzalin, C.M. and J. Lingner, *Telomere wedding ends in divorce.* Science, 2004. **304**(5667): p. 60-62.
34. Kim, M.K., C. Dudognon, and S. Smith, *Tankyrase 1 regulates centrosome function by controlling CPAP stability.* EMBO reports, 2012. **13**(8): p. 724-732.
35. Gönczy, P., *Centrosomes and cancer: revisiting a long-standing relationship.* Nature Reviews Cancer, 2015. **15**(11): p. 639-652.
36. Ozaki, Y., et al., *Poly-ADP ribosylation of Miki by tankyrase-1 promotes centrosome maturation.* Molecular cell, 2012. **47**(5): p. 694-706.
37. Guo, H.-L., et al., *The Axin/TNKS complex interacts with KIF3A and is required for insulin-stimulated GLUT4 translocation.* Cell research, 2012. **22**(8): p. 1246-1257.
38. Huang, S. and M.P. Czech, *The GLUT4 glucose transporter.* Cell metabolism, 2007. **5**(4): p. 237-252.
39. Fujita, S., et al., *Pharmacological inhibition of tankyrase induces bone loss in mice by increasing osteoclastogenesis.* Bone, 2017.
40. Berendsen, A.D. and B.R. Olsen, *Tankyrase loses its grip on SH3BP2 in cherubism.* Cell, 2011. **147**(6): p. 1222-1223.
41. Levaot, N., et al., *Loss of Tankyrase-mediated destruction of 3BP2 is the underlying pathogenic mechanism of cherubism.* Cell, 2011. **147**(6): p. 1324-1339.
42. Jia, J., et al., *Tankyrase inhibitors suppress hepatocellular carcinoma cell growth via modulating the Hippo cascade.* PloS one, 2017. **12**(9): p. e0184068.
43. Wang, W., et al., *Tankyrase inhibitors target YAP by stabilizing angiomotin family proteins.* Cell reports, 2015. **13**(3): p. 524-532.

44. Wang, H., et al., *Tankyrase inhibitor sensitizes lung cancer cells to endothelial growth factor receptor (EGFR) inhibition via stabilizing angiomotins and inhibiting YAP signaling.* Journal of Biological Chemistry, 2016. **291**(29): p. 15256-15266.
45. Li, X., et al., *Proteomic analysis of the human tankyrase protein interaction network reveals its role in pexophagy.* Cell reports, 2017. **20**(3): p. 737-749.
46. Ohishi, T., et al., *Tankyrase-binding protein TNKS1BP1 regulates actin cytoskeleton rearrangement and cancer cell invasion.* Cancer Research, 2017. **77**(9): p. 2328-2338.
47. Voronkov, A., et al., *Structural basis and SAR for G007-LK, a lead stage 1, 2, 4-triazole based specific tankyrase 1/2 inhibitor.* Journal of medicinal chemistry, 2013. **56**(7): p. 3012-3023.
48. Mariotti, L., K. Pollock, and S. Guettler, *Regulation of Wnt/β-catenin signalling by tankyrase-dependent poly (ADP-ribosyl) ation and scaffolding.* British Journal of Pharmacology, 2017.
49. Waaler, J., et al., *A novel tankyrase inhibitor decreases canonical Wnt signaling in colon carcinoma cells and reduces tumor growth in conditional APC mutant mice.* Cancer research, 2012. **72**(11): p. 2822-2832.
50. Moore, K.J., et al., *microRNAs and cholesterol metabolism.* Trends in Endocrinology & Metabolism, 2010. **21**(12): p. 699-706.
51. Kuzu, O.F., M.A. Noory, and G.P. Robertson, *The role of cholesterol in cancer.* Cancer research, 2016. **76**(8): p. 2063-2070.
52. Durand, S., et al., *A transcriptome-based protein network that identifies new therapeutic targets in colorectal cancer.* BMC genomics, 2017. **18**(1): p. 758.
53. Ikonen, E., *Cellular cholesterol trafficking and compartmentalization.* Nature reviews Molecular cell biology, 2008. **9**(2): p. 125-138.
54. Li, Y.C., et al., *Elevated levels of cholesterol-rich lipid rafts in cancer cells are correlated with apoptosis sensitivity induced by cholesterol-depleting agents.* The American journal of pathology, 2006. **168**(4): p. 1107-1118.
55. Björkhem, I., S. Meaney, and U. Diczfalusy, *Oxysterols in human circulation: which role do they have?* Current opinion in lipidology, 2002. **13**(3): p. 247-253.
56. Guo, D., et al., *Targeting SREBP-1-driven lipid metabolism to treat cancer.* Current pharmaceutical design, 2014. **20**(15): p. 2619-2626.
57. Cruz, P.M., et al., *The role of cholesterol metabolism and cholesterol transport in carcinogenesis: a review of scientific findings, relevant to future cancer therapeutics.* Frontiers in pharmacology, 2013. **4**.
58. Mollinedo, F. and C. Gajate, *Lipid rafts as major platforms for signaling regulation in cancer.* Advances in biological regulation, 2015. **57**: p. 130-146.
59. Ikonen, E., *Mechanisms for cellular cholesterol transport: defects and human disease.* Physiological reviews, 2006. **86**(4): p. 1237-1261.
60. Liscurn, L., *Cholesterol biosynthesis.* New Comprehensive Biochemistry, 2002. **36**: p. 409-431.
61. Song, B.-L., N.B. Javitt, and R.A. DeBose-Boyd, *Insig-mediated degradation of HMG CoA reductase stimulated by lanosterol, an intermediate in the synthesis of cholesterol.* Cell metabolism, 2005. **1**(3): p. 179-189.
62. Baranowski, M., *Biological role of liver X receptors.* J Physiol Pharmacol, 2008. **59**(Suppl 7): p. 31-55.
63. Eberlé, D., et al., *SREBP transcription factors: master regulators of lipid homeostasis.* Biochimie, 2004. **86**(11): p. 839-848.
64. Lu, K., M.-H. Lee, and S.B. Patel, *Dietary cholesterol absorption; more than just bile.* Trends in Endocrinology & Metabolism, 2001. **12**(7): p. 314-320.

65. Li, R., et al., *SOAP2: an improved ultrafast tool for short read alignment.* Bioinformatics, 2009. **25**(15): p. 1966-1967.
66. Mortazavi, A., et al., *Mapping and quantifying mammalian transcriptomes by RNA-Seq.* Nature methods, 2008. **5**(7): p. 621-628.
67. Tarazona, S., et al., *Differential expression in RNA-seq: a matter of depth.* Genome research, 2011. **21**(12): p. 2213-2223.
68. Foundation, T.R. *The R Project for Statistical Computing*. 2017; Available from: https://www.r-project.org.
69. Mahmood, T. and P.-C. Yang, *Western blot: technique, theory, and trouble shooting.* North American journal of medical sciences, 2012. **4**(9): p. 429.
70. Diagnostica, E. *Immunofluorescence*. 2017; Available from: http://www.eurodiagnostica.com/index.php?headId=3&pageId=3&catId=10.
71. Gustafsson, M.G., *Surpassing the lateral resolution limit by a factor of two using structured illumination microscopy.* Journal of microscopy, 2000. **198**(2): p. 82-87.
72. Maxfield, F.R. and D. Wüstner, *Analysis of cholesterol trafficking with fluorescent probes.* Methods in cell biology, 2012. **108**: p. 367.
73. Roberg-Larsen, H., et al., *Highly automated nano-LC/MS-based approach for thousand cell-scale quantification of side chain-hydroxylated oxysterols.* Journal of lipid research, 2014. **55**(7): p. 1531-1536.
74. Roberg-Larsen, H., et al., *Mass spectrometric detection of 27-hydroxycholesterol in breast cancer exosomes.* The Journal of steroid biochemistry and molecular biology, 2017. **169**: p. 22-28.
75. Software, G. *QuickCalcs*. 2017; Available from: https://www.graphpad.com/quickcalcs/.
76. Ye, S., et al., *Pleiotropy of glycogen synthase kinase-3 inhibition by CHIR99021 promotes self-renewal of embryonic stem cells from refractory mouse strains.* PloS one, 2012. **7**(4): p. e35892.
77. Mahmuda, S., *Adaptive response in cancer cell to long-term tankyrase inhibitor treatment.* Master thesis, 2016.
78. Masters, J.R., *Cell line misidentification: the beginning of the end.* Nature reviews. Cancer, 2010. **10**(6): p. 441.
79. Sohn, T.A., et al., *High-throughput measurement of the Tp53 response to anticancer drugs and random compounds using a stably integrated Tp53-responsive luciferase reporter.* Carcinogenesis, 2002. **23**(6): p. 949-958.
80. Portal, E.B.R. *Cellosaurus*. 2017; Available from: https://web.expasy.org/cellosaurus/.
81. Tanaka, N., et al., *APC mutations as a potential biomarker for sensitivity to tankyrase inhibitors in colorectal cancer.* Molecular Cancer Therapeutics, 2017: p. molcanther. 0578.2016.
82. Huang, D.W., B.T. Sherman, and R.A. Lempicki, *Systematic and integrative analysis of large gene lists using DAVID bioinformatics resources.* Nature protocols, 2009. **4**(1): p. 44-57.
83. Robertson, K.A., et al., *An interferon regulated MicroRNA provides broad cell-intrinsic antiviral immunity through multihit host-directed targeting of the sterol pathway.* PLoS biology, 2016. **14**(3): p. e1002364.
84. Brown, M.S. and J.L. Goldstein, *The SREBP pathway: regulation of cholesterol metabolism by proteolysis of a membrane-bound transcription factor.* Cell, 1997. **89**(3): p. 331-340.
85. Grimmer, S., et al., *Golgi Vesiculation Induced by Cholesterol Occurs by a Dynamin-and cPLA2-Dependent Mechanism.* Traffic, 2005. **6**(2): p. 144-156.

86. Ribas, V., C. García-Ruiz, and J.C. Fernández-Checa, *Mitochondria, cholesterol and cancer cell metabolism.* Clinical and translational medicine, 2016. **5**(1): p. 22.
87. van der Bliek, A.M., Q. Shen, and S. Kawajiri, *Mechanisms of mitochondrial fission and fusion.* Cold Spring Harbor perspectives in biology, 2013. **5**(6): p. a011072.
88. Kloudova, A., F.P. Guengerich, and P. Soucek, *The Role of Oxysterols in Human Cancer.* Trends in Endocrinology & Metabolism, 2017.
89. Nims, R.W., et al., *Sensitivity of isoenzyme analysis for the detection of interspecies cell line cross-contamination.* In Vitro Cellular & Developmental Biology-Animal, 1998. **34**(1): p. 35-39.
90. (ICLAC), I.c.l.a.c. *Register of misidentified cell lines*. 2016; Available from: http://iclac.org/databases/cross-contaminations/.
91. Ferri, M., et al., *Targeting Wnt-driven cancers: Discovery of novel tankyrase inhibitors.* European Journal of Medicinal Chemistry, 2017.
92. Chatterjee, S., et al., *Identification of novel genes and pathways regulating SREBP transcriptional activity.* PLoS One, 2009. **4**(4): p. e5197.
93. Grimmer, S., et al., *Endosome to Golgi transport of ricin is regulated by cholesterol.* Molecular biology of the cell, 2000. **11**(12): p. 4205-4216.
94. Asalla, S., et al., *Restoring Mitochondrial Function: A Small Molecule-mediated Approach to Enhance Glucose Stimulated Insulin Secretion in Cholesterol Accumulated Pancreatic beta cells.* Scientific reports, 2016. **6**: p. 27513.
95. Schroepfer, G.J., *Oxysterols: modulators of cholesterol metabolism and other processes.* Physiological reviews, 2000. **80**(1): p. 361-554.

7 Supplementary

Supplementary Figure S1. western blot analysis of SREBP

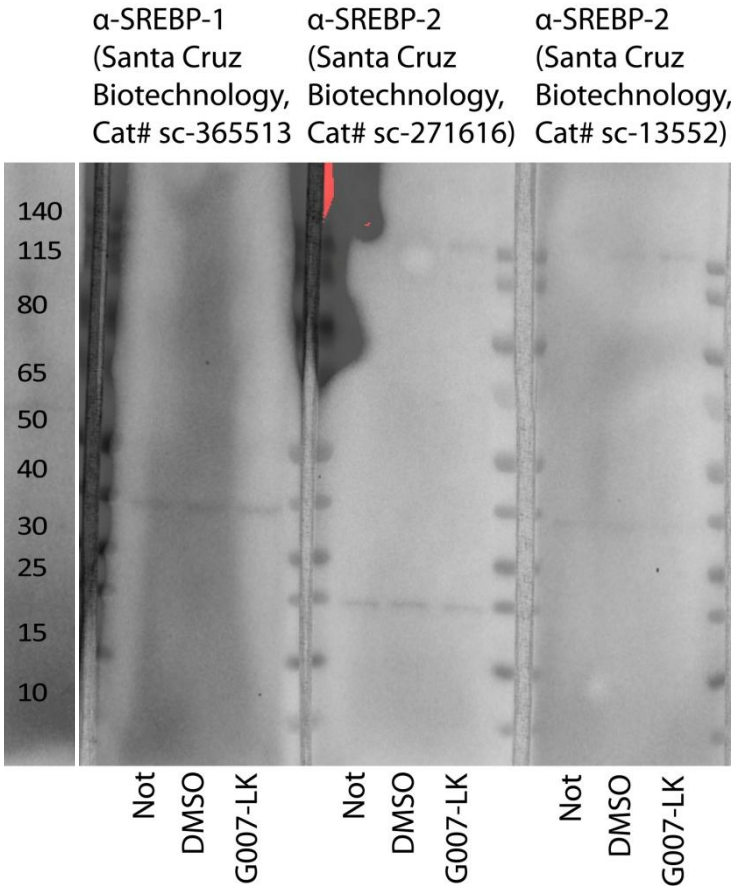

Figure S1. Western blot analysis with SREBP antibodies. Representative collection of western blot analysis using different SREBP antibodies as indicated.

Supplementary Figure 2. Complete material list

Material	Producer	Catalog nr.
Cell culturing		
ABC-1	Japanese collection of research bio resources cell bank, [JCRB cell bank]	JCRB0815
RKO	American type culture collection, [ATCC]	CRL-2577
Eagle's minimal essential medium (EMEM)	LGC-standards	30-2003
Fetal bovine serum (FBS)	Life Technologies	16141-079
Pencillin-streptomycin	Sigma Aldrich	P4333
Trypsin- Ethylenediaminetetraacetic acid (EDTA)	Sigma Aldrich	T3924
1X PBS	Ullevål universitetssykehus, mikrobiologisk avdeling	-
MycoAlert™ commercial mycoplasma detection kit	Fischer	11680271
Cell treatments		
CHIR	Selleck Chemicals	S2924
G007-LK	ChemRoyal Inc.	-
Dimethyl sulfoxide (DMSO)	Sigma Aldrich	D8418
Western blot		
Methanol	VWR	20903.368
Pierce® RIPA Buffer	Thermo Scientific	89901
cOmplete Tablets - Protease inhibitor Cocktail Tablets	Roche applied science	4693124001
PhosSTOP - Phosphatase Inhibitor Cocktail Tablets	Roche applied science	04906837001
Nu-PAGE® Tris-Acetate SDS running buffer 20X	Life technologies	LA0041
Nu-PAGE® MOPS SDS running buffer	Life Technologies	NP0001
Nu-PAGE® Novex® 3-8 % Tris-Acetate mini gels	Life Technologies	EA0375BOX
Nu-PAGE® Novex® 4-12 % Bis-Tris Protein gels, 1.0 mm 20 well	Thermo Fisher Scientific	WG1402BOX
PageRuler Prestained Protein Ladder	Thermo Fisher Scientific	26616
Immunobilon® - P^{PQ} Transfer Membranes	Merck Life Science/Millipore	ISEQ00010

Extra thick blot paper	Bio-Rad Laboratories	1703960
Nonfat dried milk	AppliChem	A0830.0500
Tris buffered saline (TBS) tablets	Medicago	09-7510-10
Kit ECL Prime Western Blotting Detection Reagent	GE Healthcare Amersham	RPN2236
Transfer buffer		
Trizma-base	Sigma Aldrich	T1503
Glycine	Sigma Aldrich	G5516-1L
Immunofluorescence		
Presisjonsdekkglass, runde	VWR	MARI0117580
Microscope slides	Marienfeld	10 002 00
ProLong™ Diamond Antifade Mountant	Thermo Fisher Scientific	P36961
Poly-lysine solution	Sigma Aldrich	P8920
Fluoroshield with DAPI	Sigma Aldrich	F6057
Triton X-100	Roche applied science	10 789 704 001
4 % PFA in PBS		
Parafromaldehyde powder	Sigma Aldrich	158127
Sodium hydroxide (NaOH)	VWR	1.06462.5000
4 % BSA in PBS		
BSA Cohn fraction V, Proteasfri	SAVEEN WERNER AS	B2000-100
Plasmid purification		
pSREBP-1a	Addgene	26801
pSREBP-1c	Addgene	26802
pSREBP-2	Addgene	26807
pSynSRE-T-Luc	Addgene	60444
pSynSRE-Mut-T-Luc	Addgene	60490
pSRE-Luciferase	ATCC	MBA-120
Luria-Bertani (LB) medium	OUS, Ullevål, Mikrobiologisk avdeling	-
QIAGEN Plasmid Midi Kit	Qiagen	12143
Plasmid transfection using FuGENE HD		
Opti-MEM	Invitrogen	31985-047
FuGENE HD	Nerlien Mezansky	E2311
Dual-Luciferase Reporter Assay		
Renilla pRL-TK Vector	Promega	E2241
Dual-Luciferase Reporter Assay 1000 assay kit	Promega Nerliens	E1980
RT-qPCR		
GenElute Mammalian Total RNA Purification Kit	Sigma Aldrich	RTN350

SuperScript VILO cDNA synthesis Kit	Life Technologies	4369510
TaqMan Gene Expression Mastermix	Life Technologies	4309849